TECHNICAL NOTE

D-1335

A LARGE-SCALE WIND-TUNNEL INVESTIGATION

OF A WINGLESS VERTICAL TAKE-OFF

AND LANDING AIRCRAFT

By David G. Koenig and James A. Brady

Ames Research Center
Moffett Field, Calif.

NATIONAL AERONAUTICS AND SPACE ADMINISTRATION

WASHINGTON February 1963

NATIONAL AERONAUTICS AND SPACE ADMINISTRATION

TECHNICAL NOTE D-1335

A LARGE-SCALE WIND-TUNNEL INVESTIGATION OF A WINGLESS VERTICAL TAKE-OFF AND LANDING AIRCRAFT

By David G. Koenig and James A. Brady

SUMMARY

An investigation of a large-scale wingless vertical take-off and landing aircraft has been conducted at zero sideslip. Data from tests made at fixed ground height are presented in a previously published report. Data from tests with the wind-tunnel ground plane are presented in this report. Most of the tests were made at airspeeds of between 0 and 70 knots, at or near values of trim lift of 1500 pounds. Tests on the ground plane system were made at three ground heights from 1.2 to 2.3 duct diameters as well as with two vertical positions of the horizontal tail.

The effectiveness of pitch and yaw control, though limited for hovering, increased rapidly with airspeed. A considerable amount of roll-yaw coupling was present in the roll control. Longitudinal stability for most of the transition airspeeds was improved by raising the horizontal tail about 0.6 of a duct diameter. Reducing ground height caused increases in required flight attitude and power and augmented unsteady aerodynamic loading for low airspeeds as well.

INTRODUCTION

The wingless aircraft has been considered a possible means of combining acceptable efficiency in high-speed flight with adequate performance stability and control characteristics during low-speed or hovering flight. Several aspects of this type of aircraft are discussed in references 1 and 2 where a performance theory based on simple momentum-energy relations is used to predict cruising efficiencies that are comparable with winged aircraft. An initial full-scale aircraft was constructed with the objective of exploring performance, stability and control characteristics in low-speed flight of a "flying duct" configuration. The aircraft is designed so that the forward duct is maintained in a near horizontal attitude for all flight speeds and the main lifting jet efflux is deflected, as required, by a system of cascaded turning vanes.

An investigation of the aerodynamic characteristics of this aircraft has been made in the Ames 40- by 80-Foot Wind Tunnel and preliminary

results have been presented in reference 3. Additional tests were made to study the effect of the presence of the ground as well as the effect of tail height. The results of these tests which were made on the wind-tunnel ground plane system are presented herein. Also presented is a brief discussion of results obtained from all the full-scale wind-tunnel tests on the aircraft.

NOTATION

c propeller blade chord, in.

C_D drag coefficient, $\frac{\text{drag}}{q_\infty S}$

C_{D_o} external drag coefficient

C_L lift coefficient, $\frac{\text{lift}}{q_\infty S}$

C_l rolling-moment coefficient about an axis parallel with free stream, $\frac{\text{rolling moment}}{q_\infty Sd}$

C_m pitching-moment coefficient, $\frac{\text{pitching moment}}{q_\infty Sd}$

C_n yawing-moment coefficient, $\frac{\text{yawing moment}}{q_\infty Sd}$

C_P power coefficient, $\frac{\text{power}}{q_\infty SV_\infty}$

d duct internal diameter, ft

D drag, lb

e ratio of main exhaust cross-sectional area to forward duct area, S

h ground height as measured to the forward duct center line, ft

L lift, lb

M pitching moment, ft-lb unless otherwise indicated

P total engine chart power, hp

q dynamic pressure, lb/sq ft

r	local radius, ft
R	duct radius, ft
S	reference area, $\left(\frac{\pi}{4}\right)d^2$, ft^2
S_j	jet efflux area (see appendix A), ft^2
S_o	area of entrained air (see appendix A), ft^2
t	propeller blade thickness, in.
T	static thrust, lb
V	airspeed, knots or ft/sec
V_j	velocity of main exhaust air, ft/sec
V_1	velocity in duct adjacent to the nacelle, ft/sec
W	weight rate of flow through forward duct, lb/sec
x	distance aft of moment center parallel to duct center line, ft
y	distance out from plane of symmetry, ft
z	distance above the extended forward duct center line, ft
α	angle of attack of the aircraft
β	propeller blade angle for given radius, r, deg
γ	effective angle between the propulsion jet exhaust stream and free stream (see appendix A), deg
δ_a	roll control deflection, deg
δ_e	elevator deflection, positive with trailing edge down, deg
δ_r	rudder deflection, deg
ϵ	downwash angle, deg
η_p	propeller efficiency, ratio of energy rate imparted to the air by the propeller to the engine power
θ	cascaded vane setting (see fig. 2(b)), deg
θ_F	forward vane setting (see fig. 2(b)), deg

λ velocity ratio, $\frac{V_j}{V_o}$ (see appendix A)

ρ free-stream density

σ stability parameter, $\frac{\partial M}{\partial \alpha} - \frac{\frac{\partial M}{\partial V_\infty} - \frac{\partial L}{\partial \alpha}}{\frac{\partial L}{\partial V_\infty}}$

φ entrainment ratio, $\frac{S_o}{S_j}$

Subscript

∞ free stream

AIRCRAFT AND TEST EQUIPMENT

A photograph of the aircraft mounted on the ground-plane support system is presented in figure 1(a). The aircraft mounted in the wind tunnel for the tests of reference 3 is shown in figure 1(b). A three-view sketch of the aircraft is presented in figure 2(a) and details of the turning vane system are shown in figure 2(b). The geometry for the propellers used in both the tests is described in figure 2(c); for additional details of the internal ducting system, as well as the elevators and rudder, see reference 3.

Slight modifications to the aircraft were made prior to the tests on the ground plane system reported herein. The structure surrounding the forward duct was strengthened and the inlet lip was reinforced to minimize deflection of the duct under load. The turning vanes and turning vane mounts were reinforced and the power absorption capacity of the propellers was increased. As an indication of the effect of the change in propeller design, typical duct velocity profiles obtained from the tests of reference 3 are presented in figure 3 together with velocity profiles measured during the ground plane tests.

The ground plane system consists of support struts with which the height of the aircraft above a fixed ground plane could be changed readily. The ground plane was installed 3 feet above the original tunnel floor in the wind-tunnel test section. Two-component load cells were mounted at each of the three support points. The longitudinal data presented in this report, namely, lift, drag, and pitching moment, were derived from the output of the load cells.

Photographs of the horizontal tail mounted in the low and high positions are presented in figures 4(a) and (b), respectively. The details of the low tail installation are described in reference 3. For the upper position, the tail had the same plan form and length as were used for the low position, but the tail was raised 0.62 duct diameters above the original position. For this tail position no jet deflector was used in front of the longitudinal control exhaust jet.

TESTS AND PROCEDURE

The series of tests on the ground plane system, for which results are presented herein, followed a procedure similar to that used for the tests of reference 3. This procedure was as follows: A trim lift was chosen which did not exceed the estimated structural limits of the aircraft (either 1500 or 2000 lb). Values of angle of attack, elevator setting, and power setting required to maintain trim lift, zero drag, and zero pitching moment were approximated by experiment. Data were then obtained with one of these three parameters as a variable while the other two were held approximately constant.

Tests were made at the high ground height, $h/d = 2.3$, for values of trim lift of 1500 and 2000 pounds and tests were made at ground heights of $h/d = 1.2$ and 1.6 for a trim lift of 1500 pounds. For the lower ground height ($h/d = 1.2$), unsteady flow obtained at an airspeed of 20 knots prevented continuous testing near trim conditions for this airspeed. Tests with the horizontal tail in the high position were made at $h/d = 1.2$ and 2.3 for four airspeed and vane setting combinations.

Data were obtained at airspeeds between 20 and 60 knots for tests at conditions near 1500 pounds lift and between 30 and 70 knots for tests in which attempts were made to trim the aircraft at 2000 pounds.

DATA REDUCTION

The C_L, C_D and C_m values presented were computed from the outputs of strain-gage load cells located at the three aircraft attachment points on the support struts. No corrections for wind-tunnel wall effects were made. However, corrections for apparent wind-stream misalinement with the tunnel walls due to the presence of the ground plane system were applied as follows. From initial directional rake measurements for corresponding values of ground height, h/d, an angle-of-attack change, $\Delta\alpha$, was chosen. For the ground heights investigated, these values of $\Delta\alpha$ were as follows.

h/d	$\Delta\alpha$, deg
1.2	2.5
1.6	2.6
2.3	2.8

The resulting corrected values of angle of attack and drag coefficient are then:

$$\alpha = \alpha_u + \Delta\alpha$$

$$C_D = C_{D_u} + C_L \sin \Delta\alpha$$

where α_u (corresponding to C_{D_u}, the drag coefficient measured in direction parallel to the walls) was the angle of attack with respect to the tunnel walls. It should be mentioned that a comparison of power-off data taken from the ground plane tests with that presented in reference 3 seems to substantiate the above values of $\Delta\alpha$.

The following are the estimated errors of measurement of both the test variables and measured values of forces and moments as based on the least count of the respective readout systems:

α	$\pm 0.2^\circ$	q	±0.02 ft lb
Lift	±10 lb	δ_e, δ_a, δ_r, θ	$\pm 1/4^\circ$
Drag	±10 lb		
Pitching moment	±80 ft lb	P	±5 hp

The values of power listed were obtained from the engine performance charts of the manufacturer as were those for the tests of reference 3. Based on past experience the values of chart powers are believed to be within 5 percent of the actual engine output.

RESULTS AND DISCUSSION

Basic Aerodynamic Characteristics

Data from tests on the ground plane system are presented in figures 5 through 10. Most of the power-on force and moment data are presented in figures 5 through 8 for the aircraft with low tail height, and in figure 9 for the high tail height. Data from the power-off tests are presented in figure 10.

Values of angle of attack, elevator setting, and power required to trim at both 1500 and 2000 pounds are listed in table II. The values were derived from data obtained during the tests by a method similar to the one used in reference 3. It should be mentioned that the data

obtained on the ground plane system at variable power or longitudinal control deflection are not presented since the rate of change of the aerodynamic coefficients with power and control setting was approximately the same as that measured in the tests of reference 3.

Some of the data presented in table II are plotted in figure 11 as a function of ground height.

Control Effectiveness

The measured values of control effectiveness are presented in table III for several of the test conditions.

Longitudinal and directional control.- It was found, as expected, that at moderate to high airspeed the longitudinal and directional control performed well as conventional elevator and rudder. However, as airspeed is reduced the values of $\partial C_m/\partial \delta_e$ and $\partial C_n/\partial \delta_r$ did not increase as much as might be expected if the portion of the control moment due to jet reaction were assumed adequate. For the longitudinal control in hovering (jet reaction), calculations of an idealized control system based on simple momentum energy considerations gave values of $\partial M/\partial \delta_e$ of about 10 times the measured values. It is believed that the major factor contributing to the large discrepancy between the calculated and measured control effectiveness was inadequate turning at the control jet exit; a system using cascaded vanes would be more effective.

Roll control.- The design of the roll control used on the aircraft was such that roll control effectiveness as well as roll-yaw coupling (about the stability axis) depends significantly on aircraft attitude and vane angle. Although the values of table III represent varying combinations of angle of attack and vane angle, it seems evident that roll control is inadequate principally at the higher airspeeds where there is no augmentation by external aerodynamic control. Simple calculations of roll control effectiveness for the hovering condition assuming uniform velocity over the lifting jet indicated that control would improve with a more efficient turning vane diffuser system producing a more uniform velocity distribution across the lift jet. At forward airspeed, roll control should be augmented by either differentially deflected elevators or roll vanes externally mounted on the forward duct.

Longitudinal Stability

As a convenience to the reader, the quasi-static transition procedures presented in reference 3 are repeated in figure 12 together with an additional procedure for constant angle of attack. As shown in figure 12(b), if the parameter $\partial M/\partial \alpha$ were used as a measure of static stability, the aircraft would be slightly unstable during transition no. 1 to an airspeed

of about 47 knots, then would become increasingly stable for increasing airspeeds above this point. This is also approximately the case if $\partial C_m/\partial C_L$ were used as a parameter as shown by the trim data of reference 3. A criterion for static stability which is probably more applicable to low-speed flight conditions is presented in reference 4; as written in dimensional form it is

$$\frac{\partial M}{\partial \alpha}\frac{\partial L}{\partial V_\infty} - \frac{\partial M}{\partial V_\infty}\frac{\partial L}{\partial \alpha} < 0$$

Defining:

$$\sigma = \frac{\partial M}{\partial \alpha} - \frac{\frac{\partial M}{\partial V_\infty}\frac{\partial L}{\partial \alpha}}{\frac{\partial L}{\partial V_\infty}}$$

values of σ were estimated for the subject aircraft for transition no. 1 and the results are presented in figure 13 together with the corresponding variation of $\partial M/\partial \alpha$. Therefore, if the stability criterion $\sigma < 0$ is valid, the aircraft would be either stable or neutrally stable throughout most of the speed range.

Effect of horizontal tail position on stability.- Downwash measurements obtained during the tests of reference 3 are presented in figure 14. The data show that destabilizing variations of ϵ with α are more severe for the lower and in-board locations ($z/d = 0.24$; $y/d = 0.44$), which are comparable to the lower tail position.

As an attempt to improve static stability for the aircraft, tests were made with horizontal tail raised to $y/d = 0.81$ for which the basic data were presented in figure 9. Values of σ could not be computed from the available test data obtained for the higher tail position; however, it is believed that $\partial M/\partial \alpha$ may be used for comparison purposes. Values of $\partial M/\partial \alpha$ are, therefore, presented in figure 15 where it is indicated for the range of airspeeds investigated, that a large improvement in stability occurred when the horizontal tail was raised.

Effects of Ground Height

The data of figure 11(a) for the low tail position show that the effect of ground height was most apparent as either the lower or higher speeds (20 and 60 knots) were approached. For 20 knots, reducing ground height from $h/d = 2.3$ to 1.6 increased the required power by about 12 percent and increased angle of attack required for trim from 4.5° to 11.5°. As has been mentioned, during the tests at these speeds of from 20 to 30 knots for the lower ground heights, the aircraft was undergoing extreme

oscillations in loading. It is believed that these oscillations were caused by random recirculation of the exhaust efflux through the forward duct inlet. Although no hovering tests were made at the lower ground heights for verification, it seems likely that recirculation would increase as the airspeed is reduced to zero and aircraft load oscillations might occur which would be difficult to control.

For the higher airspeeds and low tail height, reducing ground height (except for 30 knots between $h/d = 2.3$ and $h/d = 1.6$) tended to reduce required power somewhat so that at 60 knots, reducing ground height from 2.3 to 1.2 resulted in 20 percent less required power.

Hovering

The variations of static thrust and hovering figure of merit are presented in figure 16 for $\theta = 70^{\circ}$ and $\alpha = 20^{\circ}$. The data were obtained from the tests described in reference 3. The figure of merit was calculated with an exit area to fan area ratio of 1.54. The hovering data measured in the wind tunnel have not been shown to be close to free air values; however, the low values of figure of merit from 0.3 to 0.4 which existed for the thrust range investigated indicate that considerable improvements could probably be made with refinement in both propeller design and turning vane installation.

Forward Flight Performance

Reference 2 describes a theory used as a basis for deriving the efficiency of a simple lifting duct in forward flight. A brief summary of this theory is presented in appendix A and calculated values of L/D and jet deflection angle, γ, are presented in figure 17 for several values of the parasite drag coefficient, C_{D_o}, and the entrainment ratio, φ.

As a means of comparing the performance of the test aircraft with the theory representing performance of a simple lifting duct, results for $V_\infty = 60$ knots, $\theta_F = 31^{\circ}$, $\alpha = 0^{\circ}$, and $\theta = 33^{\circ}$ are also plotted in figure 17 with the theoretical data. The value of L/D was calculated from the results reported in reference 3 with the use of tail-off data as follows:

$$\frac{L}{D} = \frac{C_L}{\left(\frac{550\ P\eta_p}{q_\infty S V_\infty}\right) + C_D}$$

The value of η_p was estimated from rake measurements behind the forward propeller. The experimental value of C_L presented was based on an area which was 17 percent larger than the reference area, S, in order to approximate a value of S_j for the test aircraft.

Within the estimated accuracy of the test results the placement of the test point on the theoretical curves of figure 17(a) demonstrates an equivalent value of φ for the aircraft to be between 0 and 1. With the placement of the test point on figure 17(b) a value of C_{D_o} in the order of 0.2 is indicated. The comparison further demonstrates that if the relatively high value of external drag were reduced, small jet deflection angles would have to be used to achieve high L/D.

CONCLUSIONS

From the results of the investigation, the following conclusions were made concerning the control, stability, and performance of the subject aircraft.

1. Pitch and yaw control effectiveness for hovering flight was low probably because of poor control jet turning efficiency. As forward speed is attained, the conventional elevator and rudder become effective as longitudinal and directional controls. Roll control is complicated by a large amount of roll-yaw coupling and appears marginal for hovering and inadequate for forward flight.

2. Transition from hovering to forward flight appears possible with a number of different airspeed and attitude combinations.

3. Static longitudinal stability was improved when the tail position was raised.

4. For low-speed flight, reductions of ground height from 2.3 to 1.2 duct diameters increased the flight attitudes and power required for trim and augmented unsteady aerodynamic loading.

Ames Research Center
National Aeronautics and Space Administration
Moffett Field, Calif., May 14, 1962

APPENDIX A

THEORETICAL PERFORMANCE OF A PROPULSION DUCT IN FORWARD FLIGHT

Fundamentals of the theory of references 1 and 2 may be summarized as follows.

In the case where the air flow through a lifting duct is expelled at uniform velocity, V_j, and area, S_j, the jet entrains a mass of air moving at velocity $V_o = V_\infty$ with cross-section area, S_o, as shown in the following sketch:

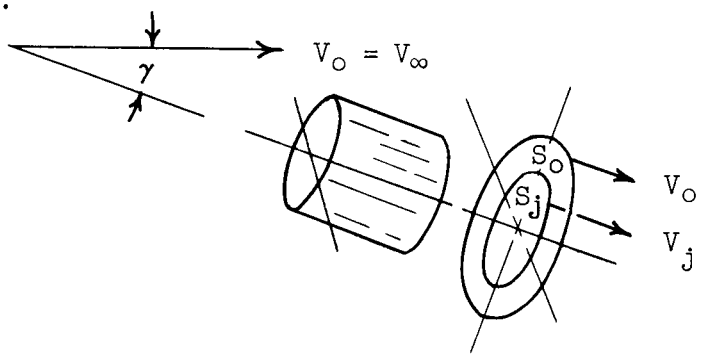

Summations of the lift and horizontal forces, L and X, respectively, are:

$$L = \sin \gamma(m_j V_j + m_o V_o) \tag{A1}$$

$$X = m_j(V_o - V_j \cos \gamma) + m_o V_o(1 - \cos \gamma) \tag{A2}$$

and the rate of change of kinetic energy in the propulsive jet is:

$$P = \frac{m_j}{2}(V_j^2 - V_o^2) \tag{A3}$$

where m_j and m_o are the mass rates of flow of the propulsive stream and the entrained stream, respectively. When the following definitions are used:

$$C_X = \frac{X}{q_\infty S_j}$$

$$C_L = \frac{L}{q_\infty S_j}$$

$$C_P = \frac{\text{kinetic energy}}{q_\infty V_\infty S_j}$$

$$C_{D_o} = \text{parasite drag coefficient}$$

equations (A1), (A2), and (A3) become:

$$C_L = 2 \sin \gamma(\lambda^2 + \varphi) \tag{A4}$$

$$C_X = 2\left[\lambda(1 - \lambda \cos \gamma) + \varphi(1 - \cos \gamma)\right] + C_{D_o} \tag{A5}$$

$$C_P = \lambda(\lambda^2 - 1) \tag{A6}$$

where $\lambda = V_j/V_o$ and $\varphi = S_o/S_j$.

It may be further shown for the condition of level flight where $C_X = 0$, that:

$$\lambda = \frac{1}{2} \cos \gamma \left\{ 1 + \sqrt{1 + 4 \cos \gamma \left[(1 - \cos \gamma) + \frac{C_{D_o}}{2} \right]} \right\} \tag{A7}$$

By the use of equations (A4), (A6), and (A7), values of γ and C_L/C_P may be computed as functions of the speed parameter $1/\sqrt{C_L}$ for assumed values of entrainment ratio φ and parasite drag, C_{D_o}.

This method was used to obtain the theoretical values presented in figures 17(a) and 17(b).

REFERENCES

1. Lippisch, A. M.: Performance Calculation of Aerodyne Systems in Cruising Flight. Collins Radio Company, Cer 617, 1957.

2. Lippisch, A. M.: Research in the Field of Wingless VTOL Aircraft. Collins Radio Company, Ctr-204, 1958. Also, IAS Preprint 808, 1958.

3. Koenig, David G., and Brady, James A.: Large-Scale Wind-Tunnel Tests of a Wingless Vertical Take-Off and Landing Aircraft - Preliminary Results. NASA TN D-326, 1960.

4. Etkin, Bernard: Dynamics of Flight: Stability and Control. John Wiley and Sons, 1959, p. 216.

TABLE I.- GEOMETRIC DATA

Duct area (including nacelle), sq ft	44.18
Duct area (excluding nacelle), sq ft	37.12
Internal diameter, ft (average)	7.50
Exhaust area (in plane 30° from reference plane), sq ft	58.0
Maximum width, ft	9.17
Moment center (distance from duct L.E.), ft	10.83
Horizontal tail	
Span, ft	18.58
Area (extended to plane of symmetry), sq ft	100.6
Aspect ratio	3.43
Taper ratio	0.438
Incidence of lower surface, deg	0
Elevator area, sq ft	59.5
Elevator hinge to moment center, ft	26.83
Rudder area, sq ft	27.0
Rudder hinge to moment center, ft	25.26
Roll-control area, sq ft	11.55
Engines, (two) Lycoming O-435-17, hp	265
Propeller diameter, ft	7.35

TABLE II.- VALUES OF ANGLE OF ATTACK, ELEVATOR SETTING, AND POWER REQUIRED TO TRIM THE AIRCRAFT; AIRCRAFT MOUNTED ON THE GROUND PLANE SYSTEM

V_∞, knots	θ_F, deg	θ, deg	h/d	α, deg	δ_e, deg	P, hp	Figure
Low tail position; lift = 1500 lb							
20	66	72	2.3	4.6	-19.3	397	5
			1.6	11.6	-29.3	450	5
30	66	50	2.3	9.0	-6.0	301	6(a)
			1.6	9.6	-6.5	311	6(a)
			1.2	10.0	-9.7	292	6(a)
30	66	55	2.3	5.4	-7.8	335	6(b)
			1.6	6.5	-7.0	348	6(b)
			1.2	8.0	-8.8	309	6(b)
40	66	50	2.3	1.7	-3.0	380	7(a)
		49-1/4	1.6	1.6	-2.9	353	7(a)
		50	1.2	.9	-2.8	349	7(a)
40	66	46	2.3	5.2	-3.0	327	Not presented
		42	1.6	5.8	-3.2	306	Not presented
		47-1/2	1.2	2.8	-3.2	325	Not presented
40	31	45	2.3	8.4	-1.6	315	Not presented
		50		6.1	-1.6	332	7(b)
		43	1.6	7.5	-1.2	293	Not presented
		49-1/4		5.6	-2.8	335	7(b)
40	31	40	1.2	10.0	-2.3	244	Not presented
		49-1/2		5.1	-2.3	314	7(b)
30	31	50	2.3	15.3	4.2	303	Not presented
		55		11.1	-1.6	330	Not presented
60	31	33	2.3	1.7	-1.0	361	8(a)
			1.6	1.8	-1.1	323	8(a)
			1.2	.6	.2	308	8(a)

V_∞, knots	θ_F, deg	θ, deg	h/d	α, deg	δ_e, deg	P, hp	Figure
Low tail position; lift = 2000 lb							
30	66	55	2.3	8.2	-7.5	513	6(b)
		60		4.8	-12.2	538	Not presented
		55	1.6	10.8	-10.1	473	6(b)
40	66	50	2.3	6.6	-3.9	528	7(a)
		55		3.2	-4.7	600	Not presented
		50	1.6	6.3	-2.4	527	7(a)
	31	50	2.3	10.1	-1.8	467	Not presented
		55		7.1	-2.1	594	Not presented
50	31	45	2.3	6.2	-1.4	507	Not presented
		50		3.2	-2.4	537	Not presented
60	31	33	2.3	6.3	-1.6	467	8(b)
70	31	32-1/2		1.8	-1.0	521	8(b)
High tail position; lift = 1500 lb							
30	66	49-1/2	2.3	10.8	-4.8	333	9(a)
		52		8.5	-5.9	309	9(a)
		49-1/2	1.2	12.6	-8.2	289	9(a)
40	66	45	2.3	6.3	-2.9	343	9(b)
		49-3/4		2.7	-1.9	392	9(b)
		49-1/2	1.2	2.7	-3.1	370	9(b)
	31	45	2.3	9.3	-1.8	337	9(c)
		50		7.2	-1.2	357	9(c)
		50	1.2	5.6	-2.0	319	9(c)
50	31	33	2.3	7.9	-1.0	299	9(d)
60	31	33	2.3	2.0	1.1	359	9(d)
			1.2	1.0	1.7	323	9(d)

TABLE III.- MEASURED CONTROL FORCES

Elevator control effectiveness				
V_∞	P, hp	θ	θ_F	$\partial C_m/\partial \delta_e$
Forward flight				
20	350	60	66	-0.40
30	336	50	66	-.35
40	330	33	31	-.36
50	309	33	31	-.34
60	372	33	31	-.32
70	345	33	31	-.32
Hovering				
0	378	70	66	$\partial M/\partial \delta_e$ = -72, ft-lb/deg

V, knots	P, hp	α, deg	θ, deg	θ_F, deg	Roll control effectiveness[1]		Rudder effectiveness[1]	
					$\partial C_l/\delta_a$	$\partial C_n/\delta_a$	$\partial C_l/\partial \delta_r$	$\partial C_n/\partial \delta_r$
Forward flight								
20	332	8	65	66	0.063	0.033	0	0.160
30	348	0	60	66	.018	.022	-.032	.155
40	353	5	50	31	.015	.015	-.003	.130
50	322	2	40	31	.008	.010		
60	380	0	33	31	.006	.010	-.018	.115
70	348	-2	33	31			-.015	.110

[1]Measured about stability axis.

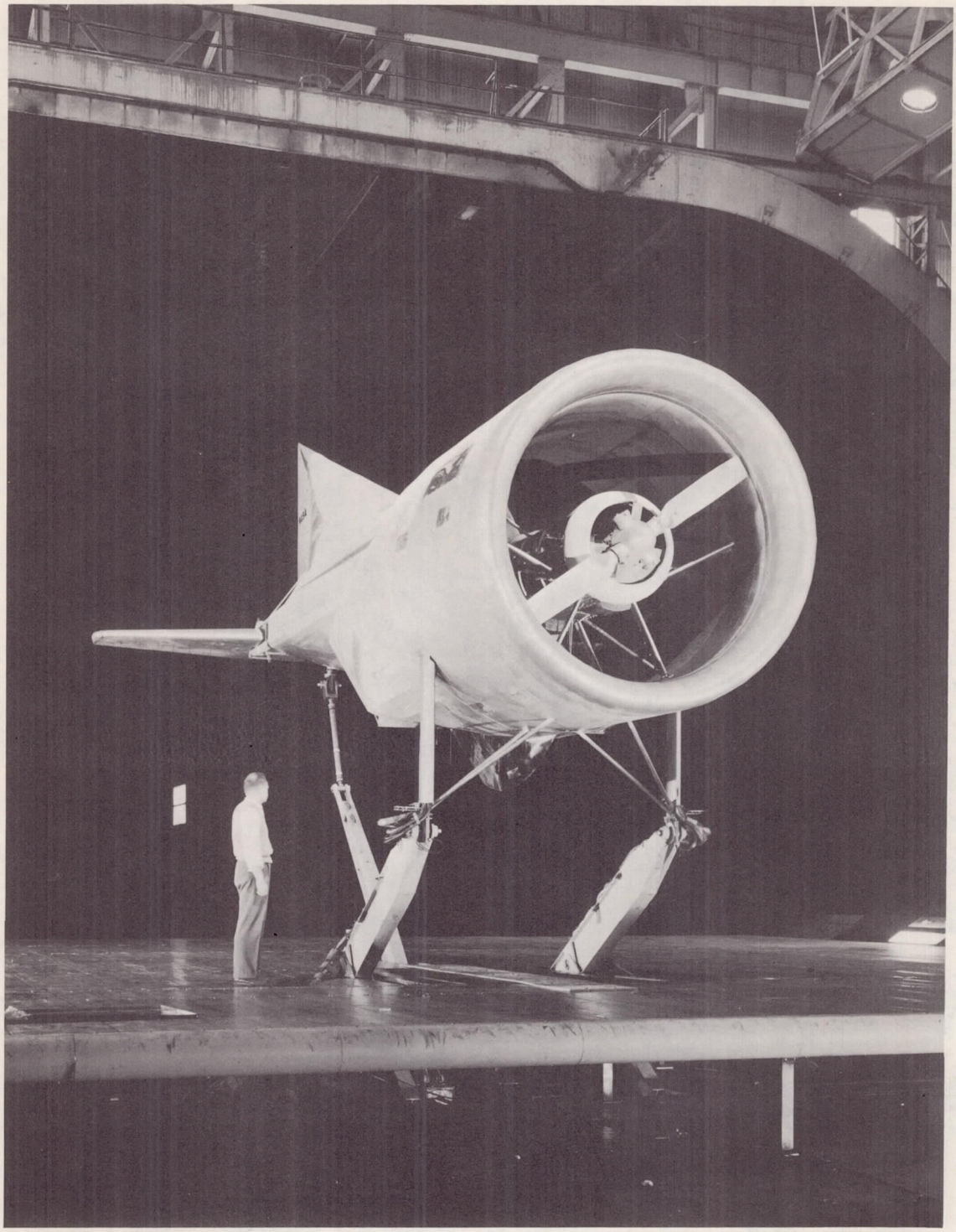

A-26150

(a) The aircraft on the wind-tunnel ground plane system.

Figure 1.- The aircraft as mounted in the Ames 40- by 80-Foot Wind Tunnel.

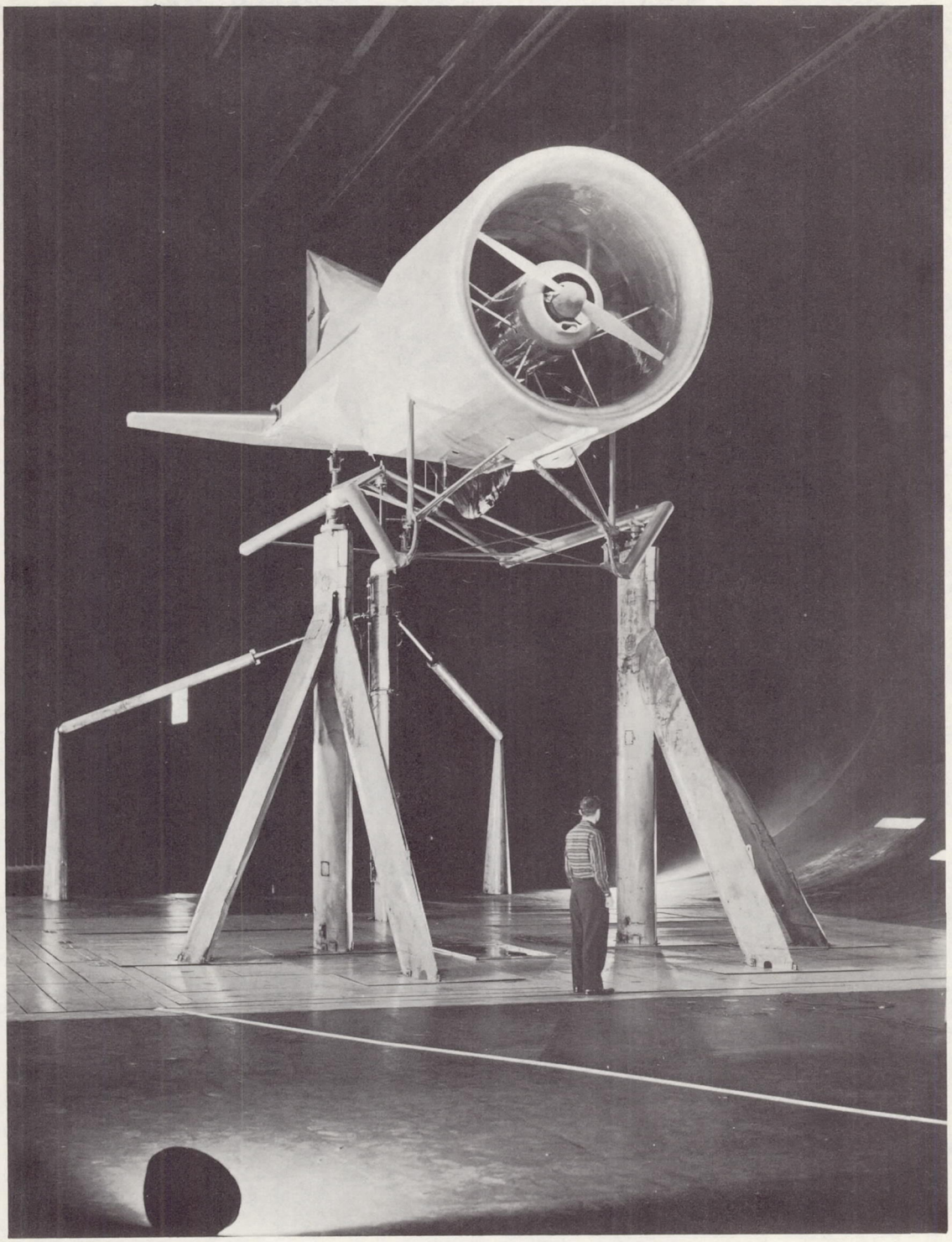

A-25698

(b) The aircraft mounted for the tests reported in reference 3.

Figure 1.- Concluded.

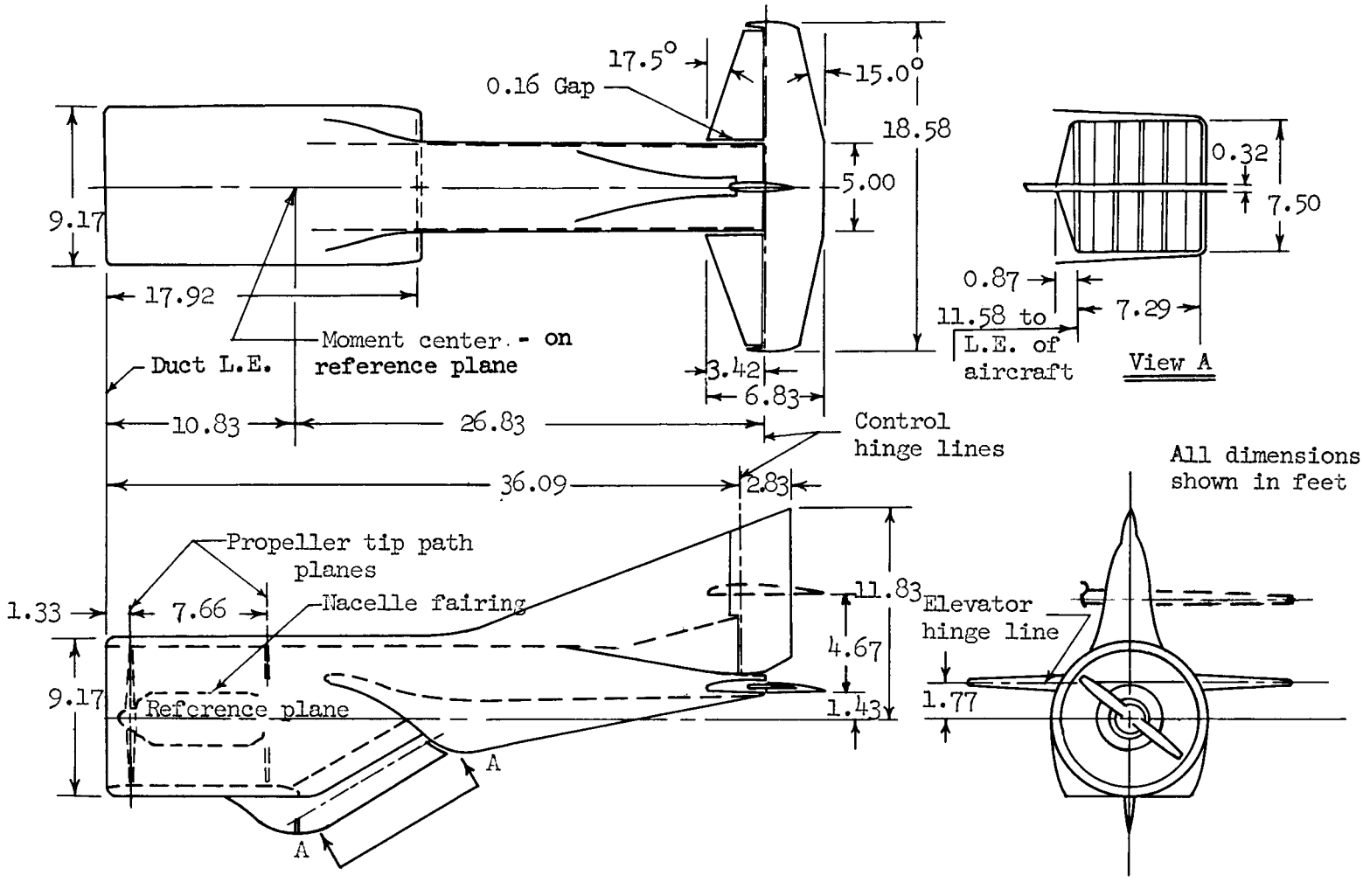

(a) Sketch of the aircraft.

Figure 2.- Geometric details of the model.

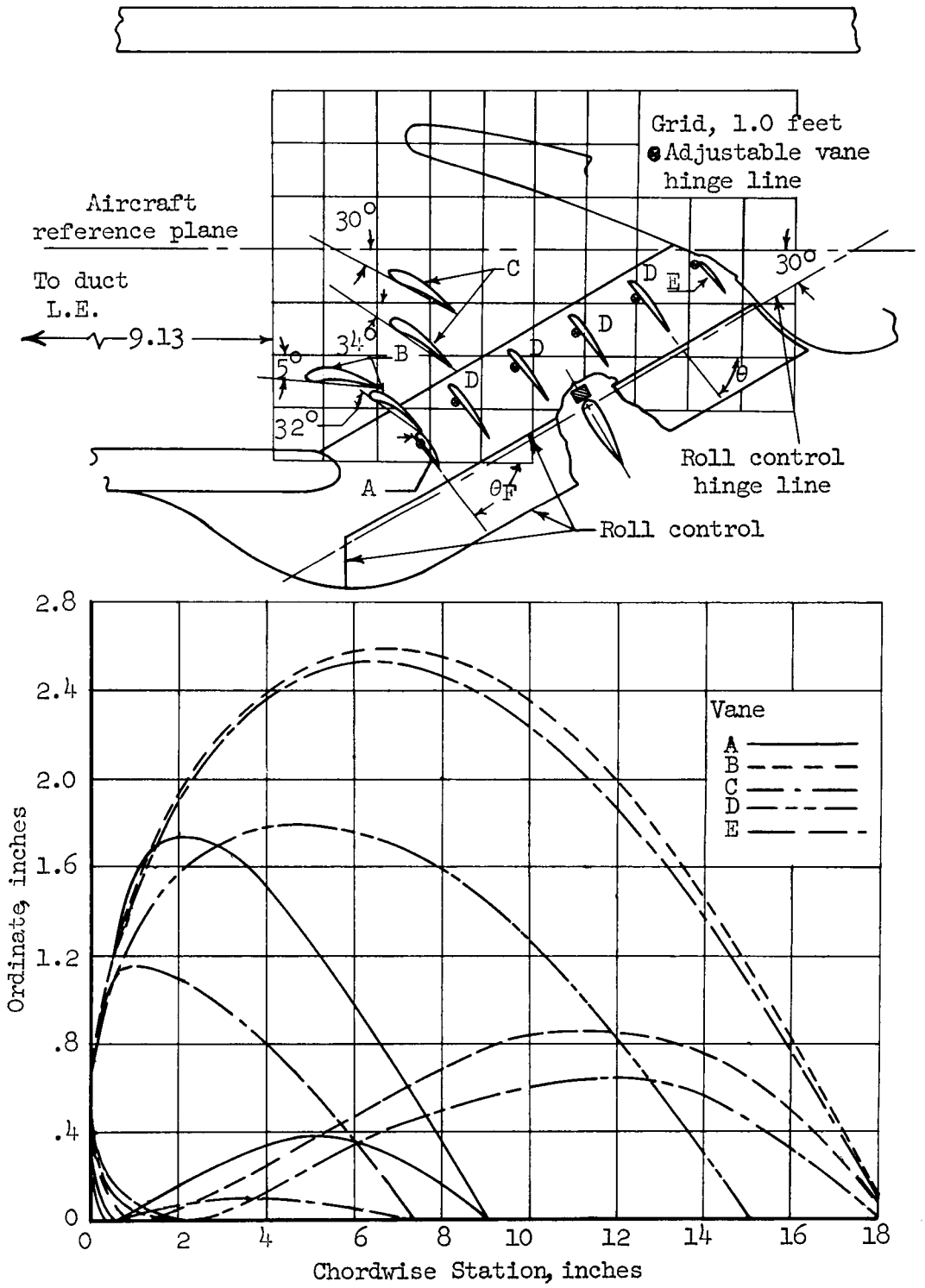

(b) Details of turning vane system and roll vane.

Figure 2.- Continued.

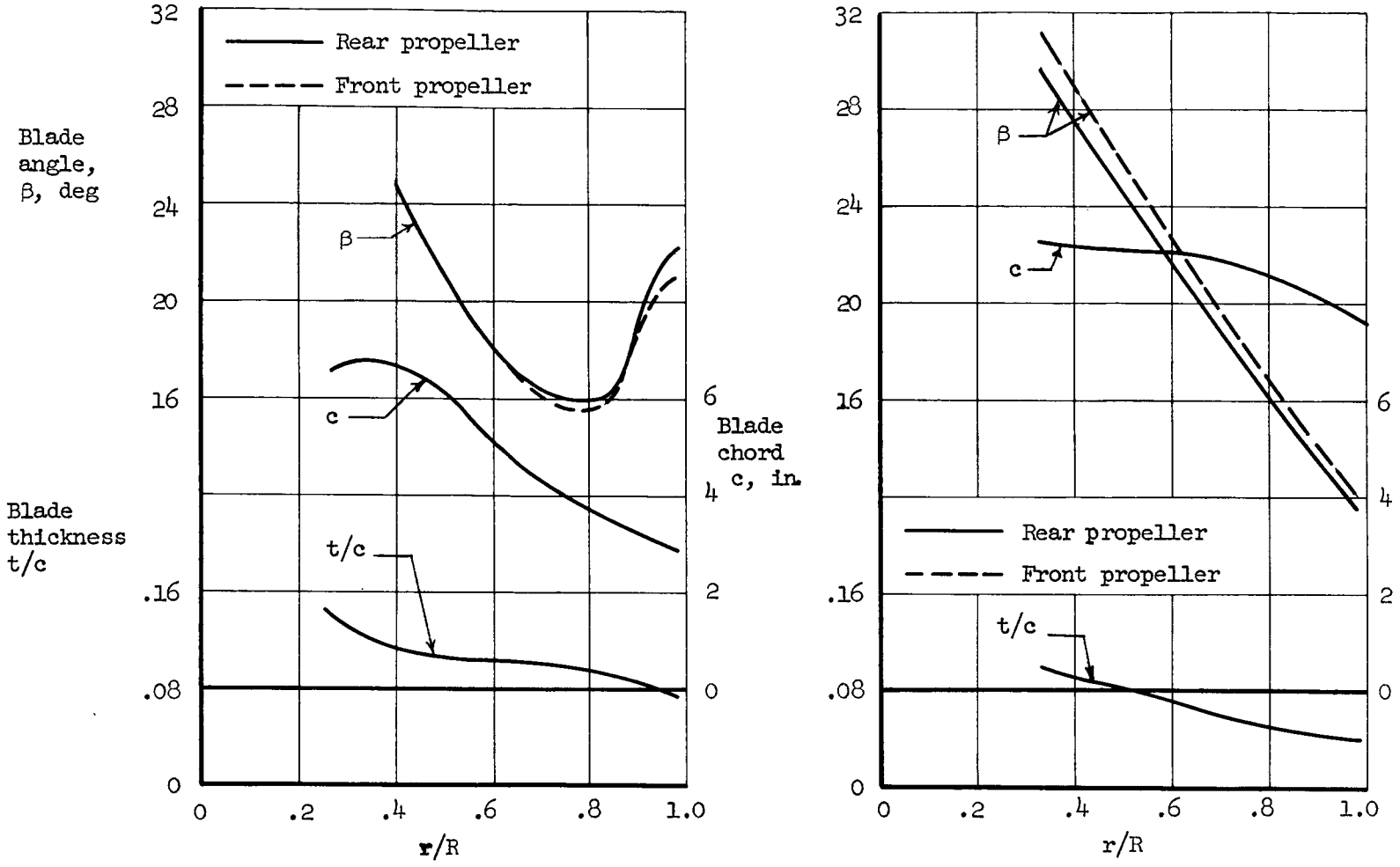

Tests of reference 3.

Tests on ground plane.

(c) Propeller configurations.

Figure 2.- Concluded.

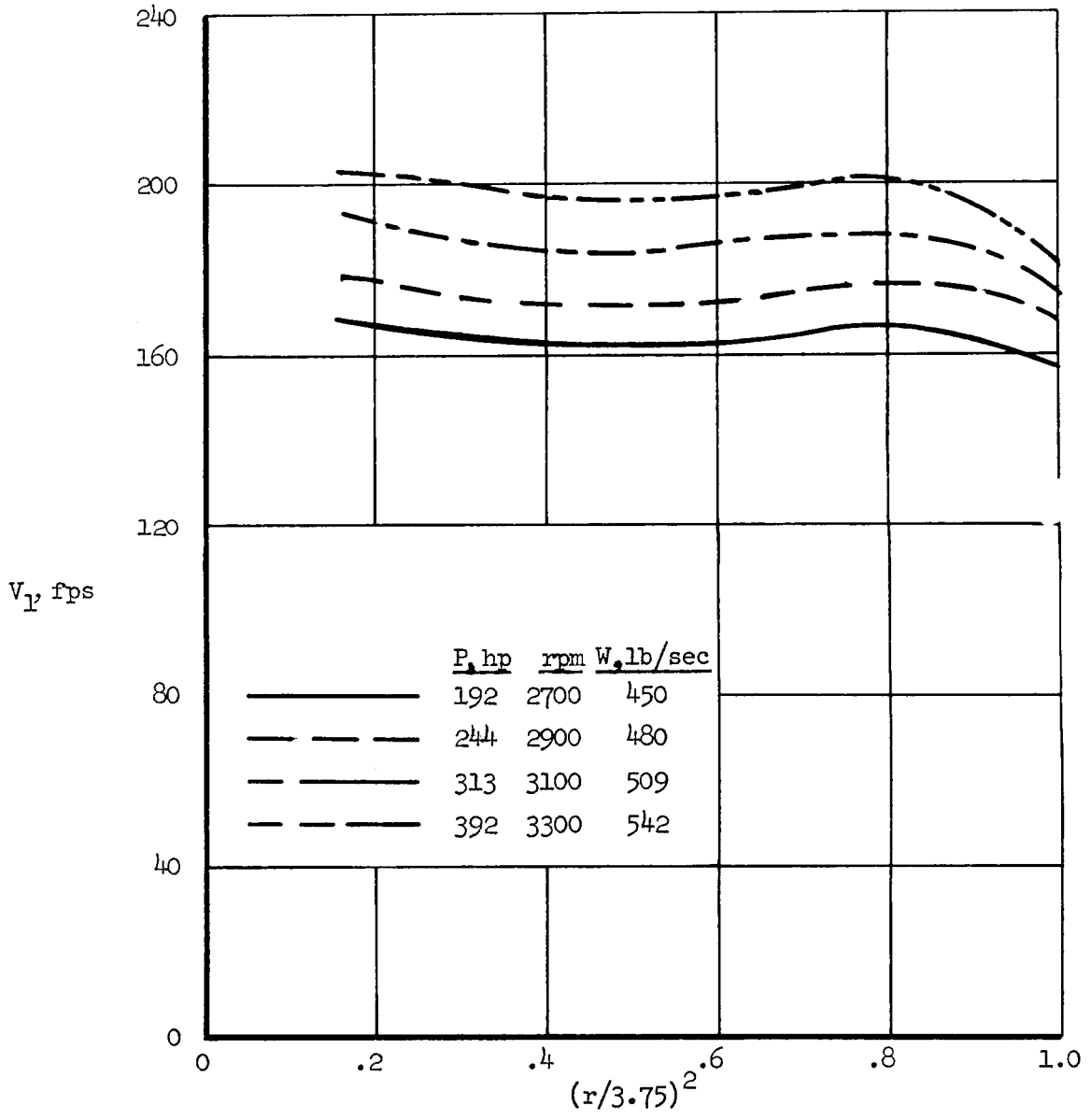

(a) Aircraft described in reference 3.

Figure 3.- The variation of velocity between the propellers with distance out from the duct center line.

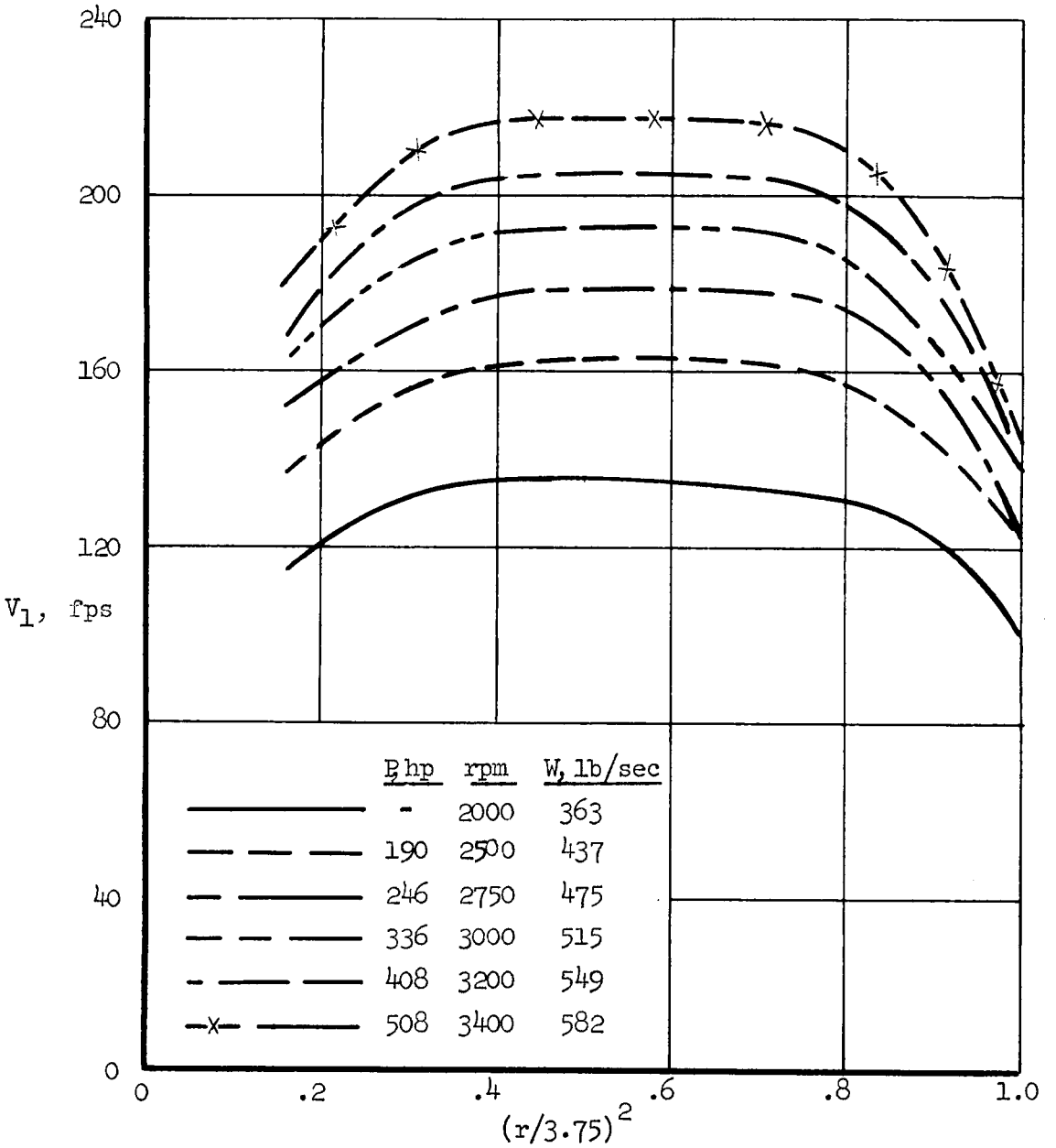

(b) Aircraft used in the tests on the ground plane.

Figure 3.- Concluded.

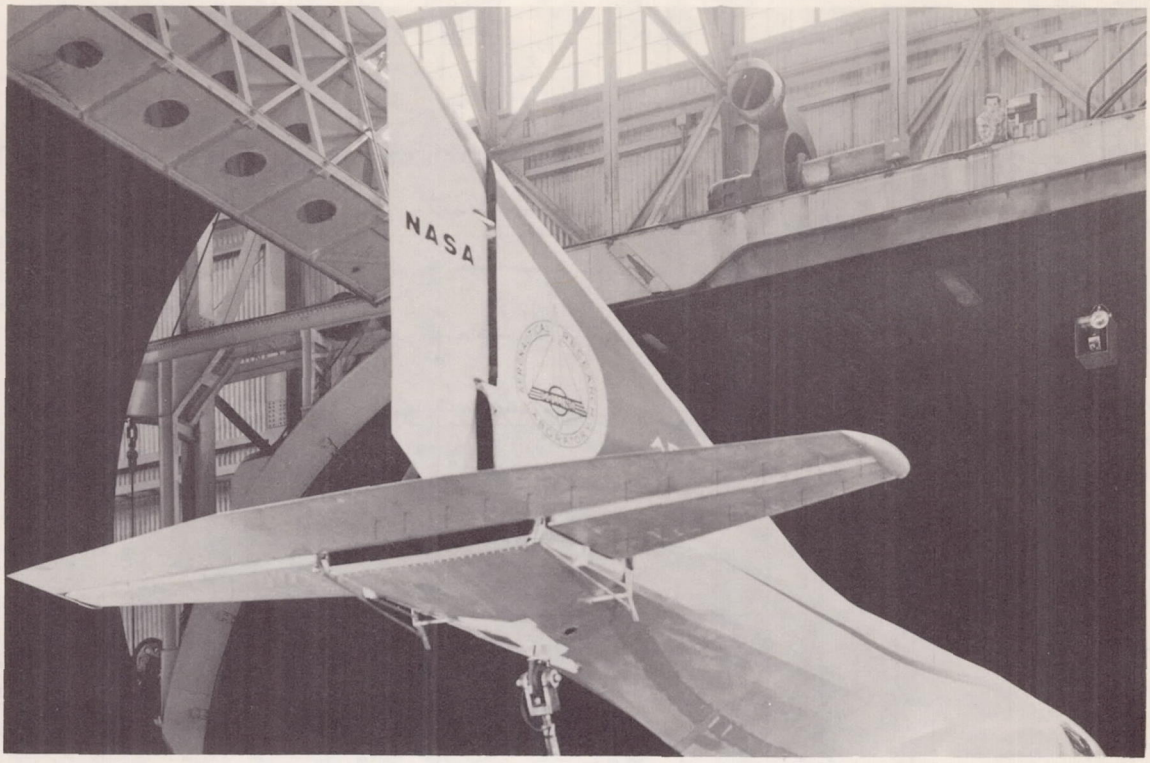

(a) Lower position z/d = 0.19. A-26151

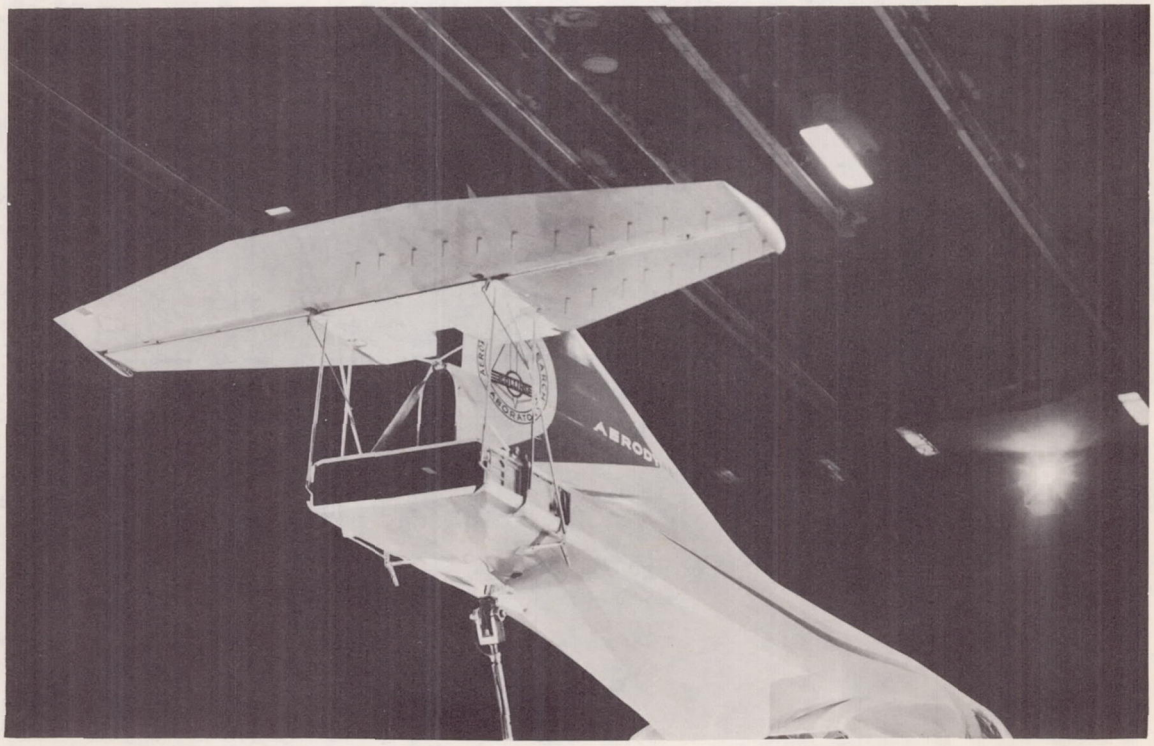

(b) High position z/d = 0.81. A-26173

Figure 4.- The horizontal-tail installation.

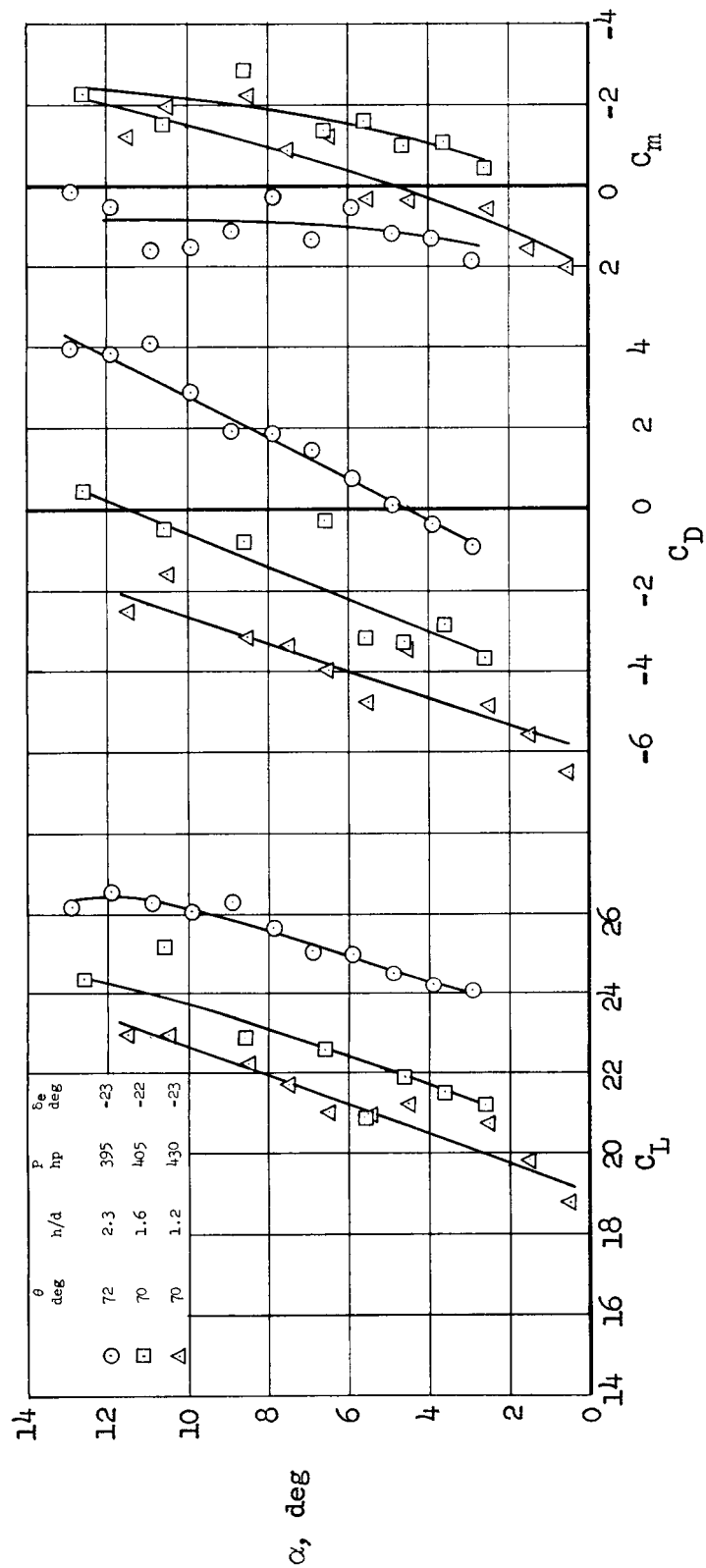

Figure 5.- Characteristics of the aircraft with the horizontal tail in the low position for V_∞ = 20 knots; θ_F = 66°.

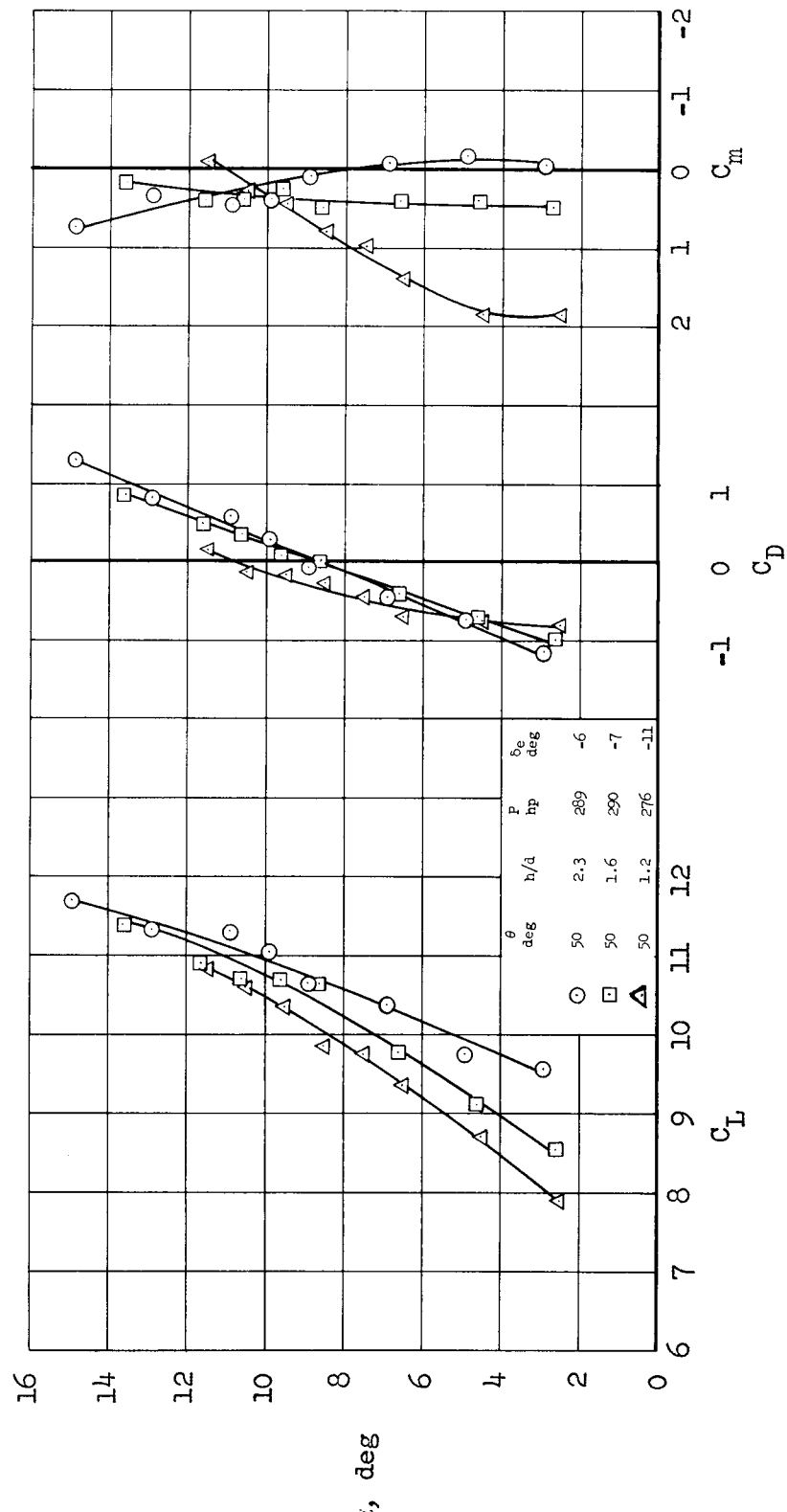

(a) $\theta = 50^\circ$

Figure 6.- Characteristics of the aircraft with the horizontal tail in the low position for $V_\infty = 30$ knots; $\theta_F = 66^\circ$.

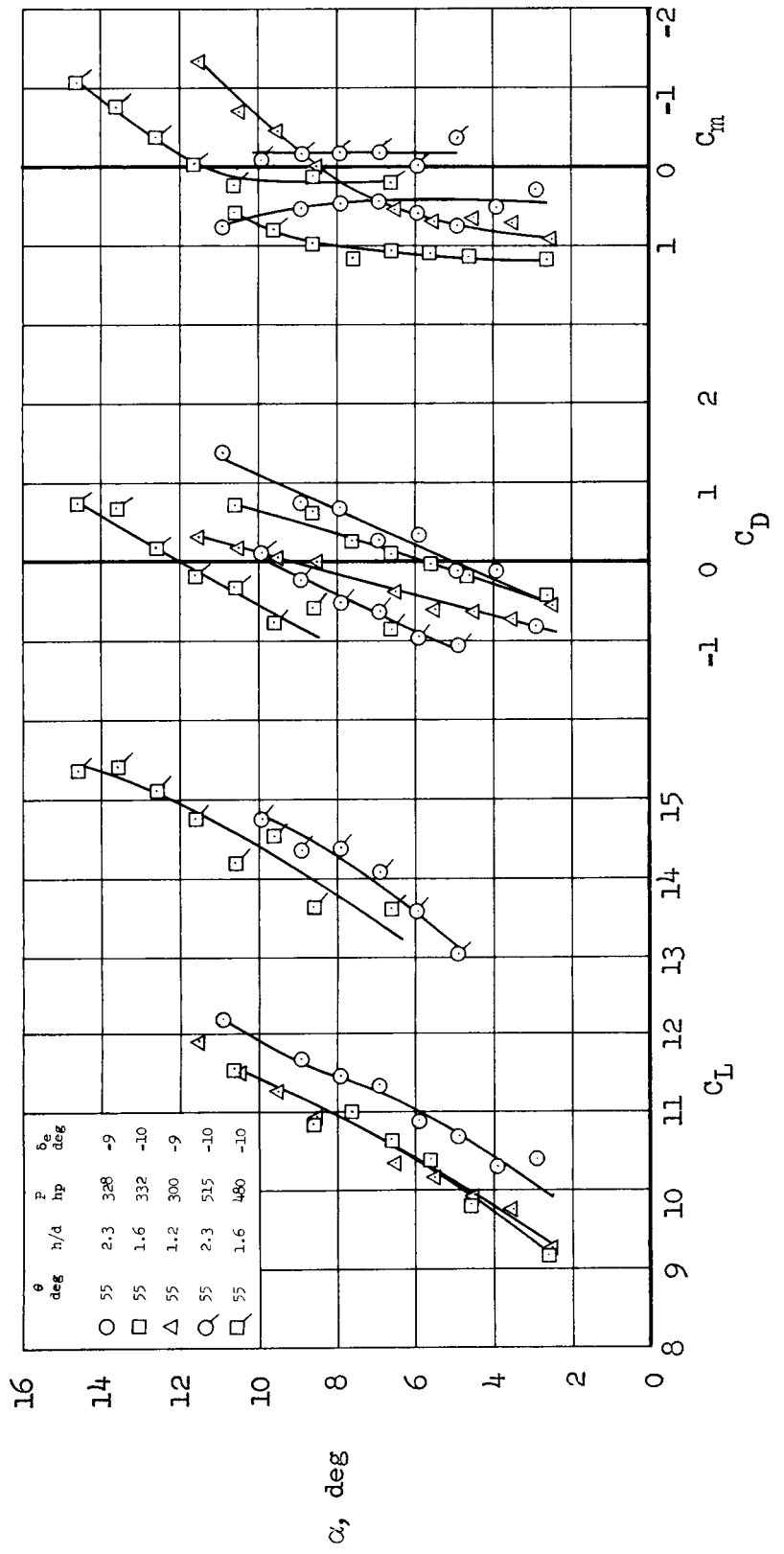

(b) $\theta = 55^{\circ}$

Figure 6.- Concluded.

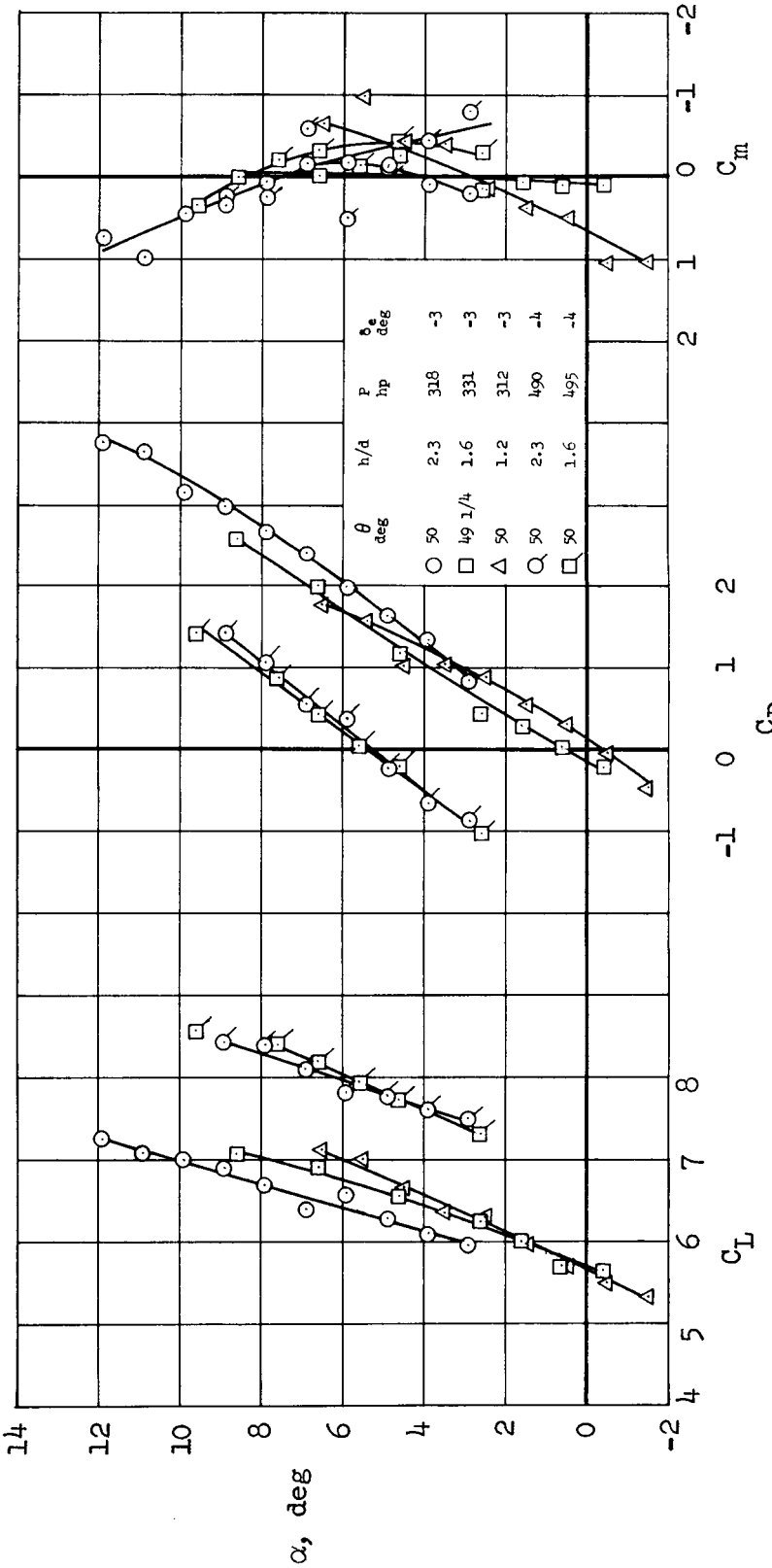

(a) $\theta_F = 66^\circ$

Figure 7.- Characteristics of the aircraft with the horizontal tail in the low position for V_∞ = 40 knots.

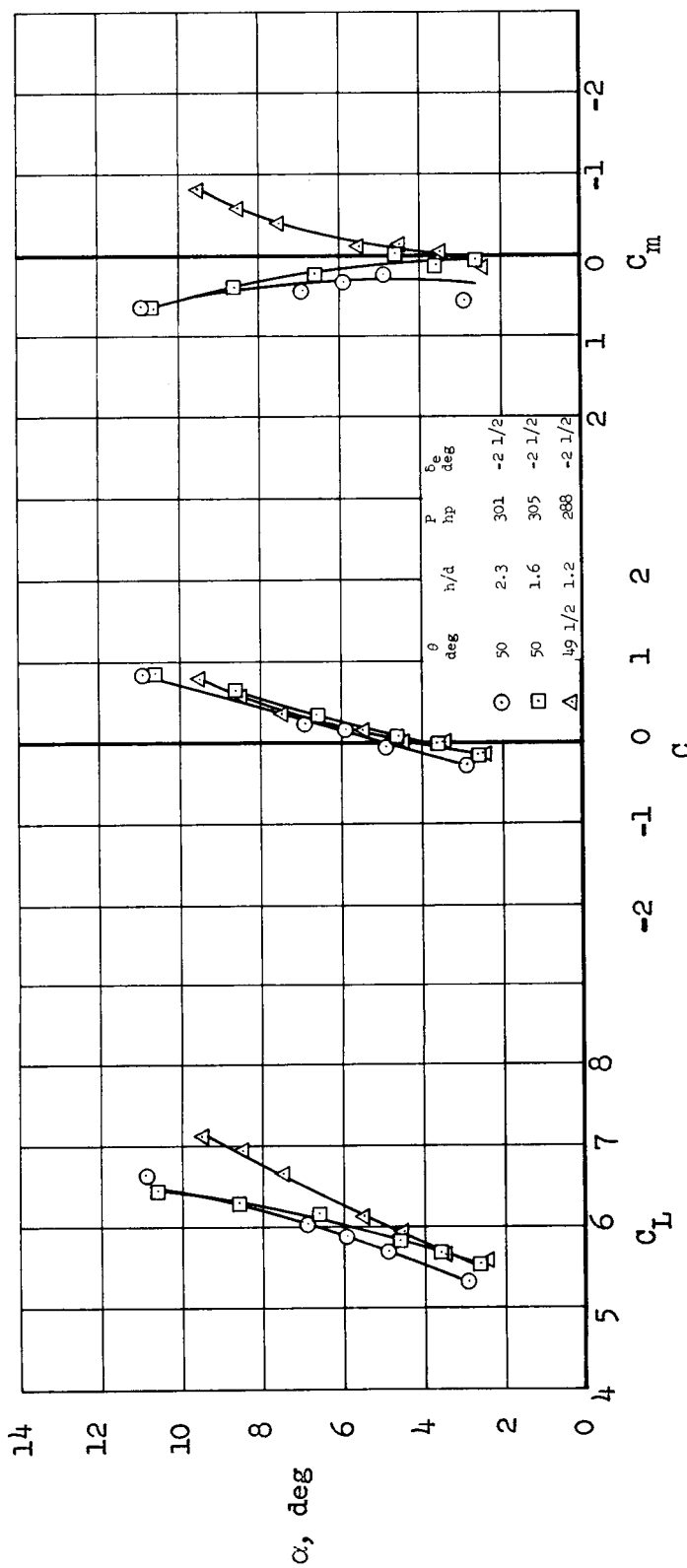

(b) $\theta_F = 31^\circ$

Figure 7.- Concluded.

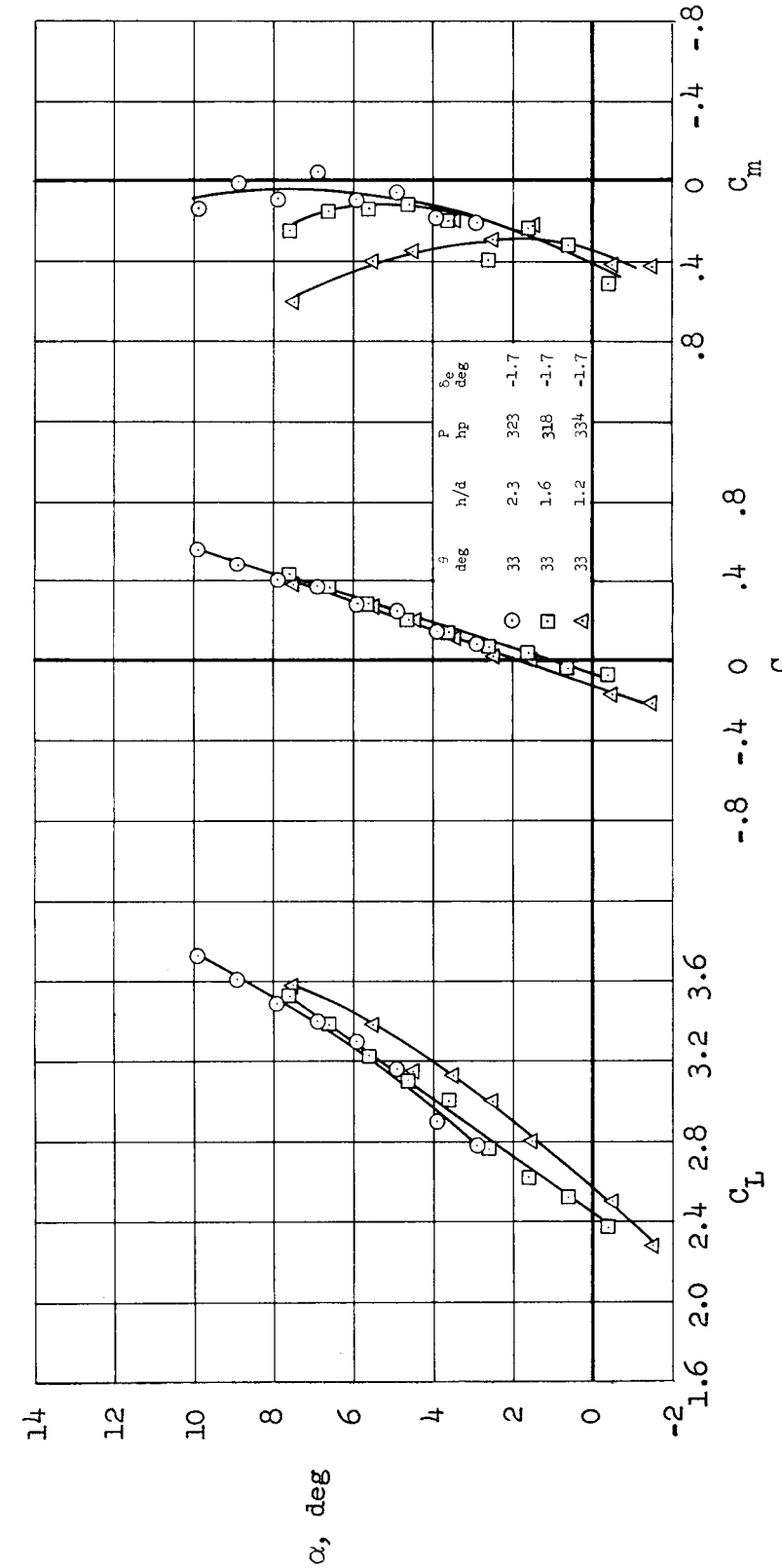

(a) Data near 1500 pounds trim lift; V_∞ = 60 knots.

Figure 8.- Characteristics of the aircraft with the horizontal tail in the low position for V_∞ = 60 and 70 knots; $\theta_F = 31^\circ$.

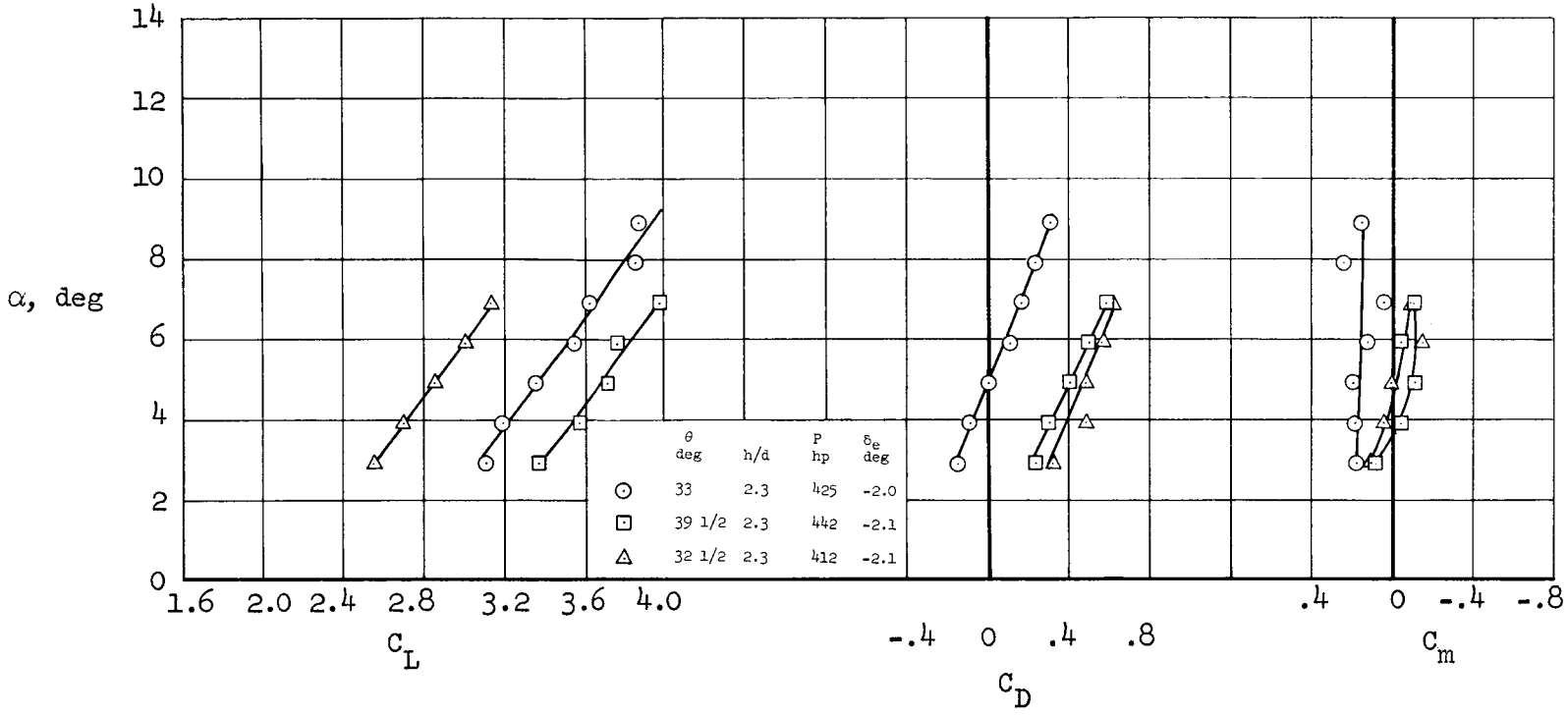

(b) Data near 2000 pounds trim lift.

Figure 8.- Concluded.

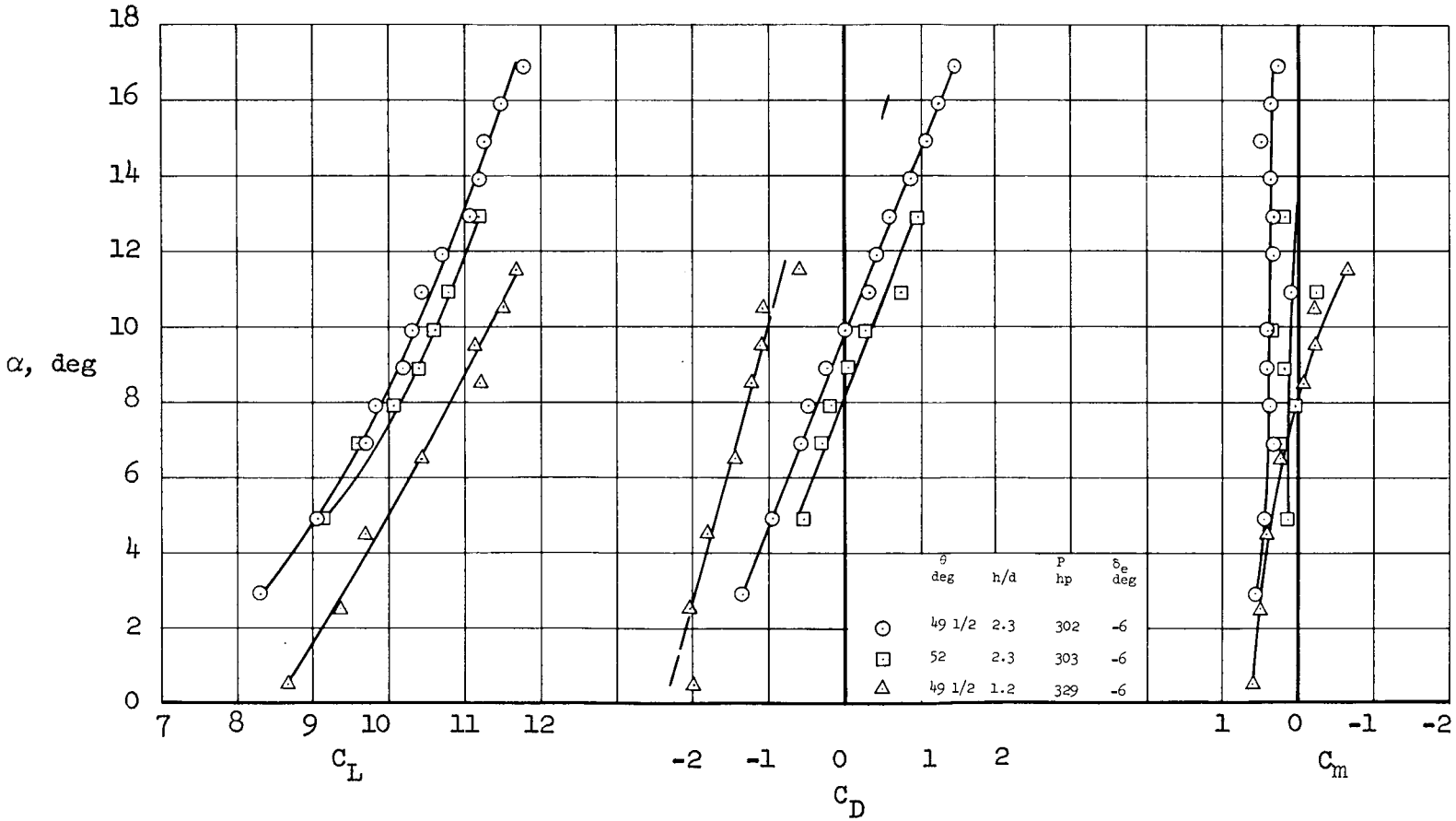

(a) V_∞ = 30 knots; $\theta_F = 66^\circ$.

Figure 9.- Characteristics of the aircraft with the horizontal tail in the high position.

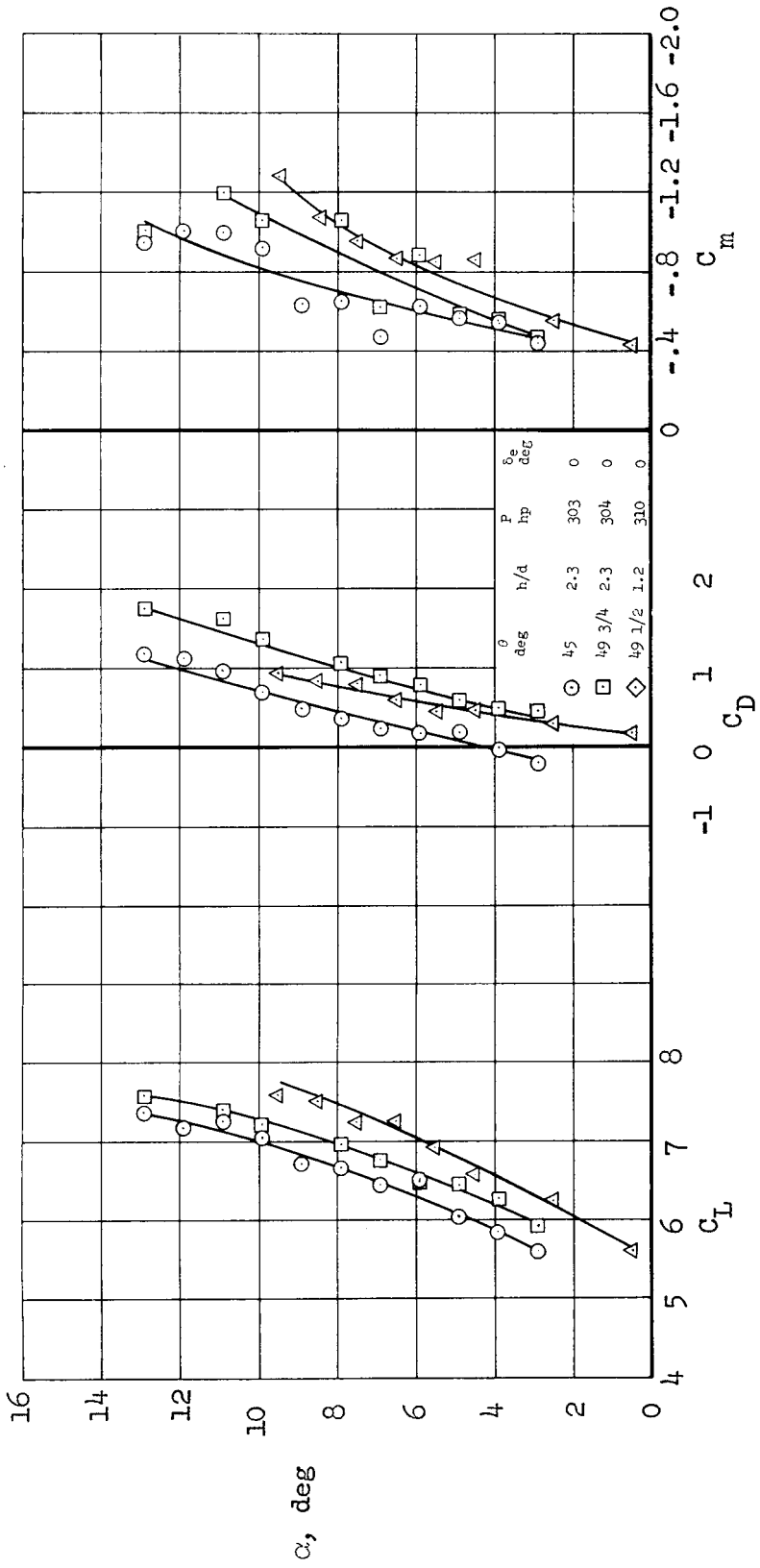

(b) V_∞ = 40 knots; $\theta_F = 66^\circ$.

Figure 9.- Continued.

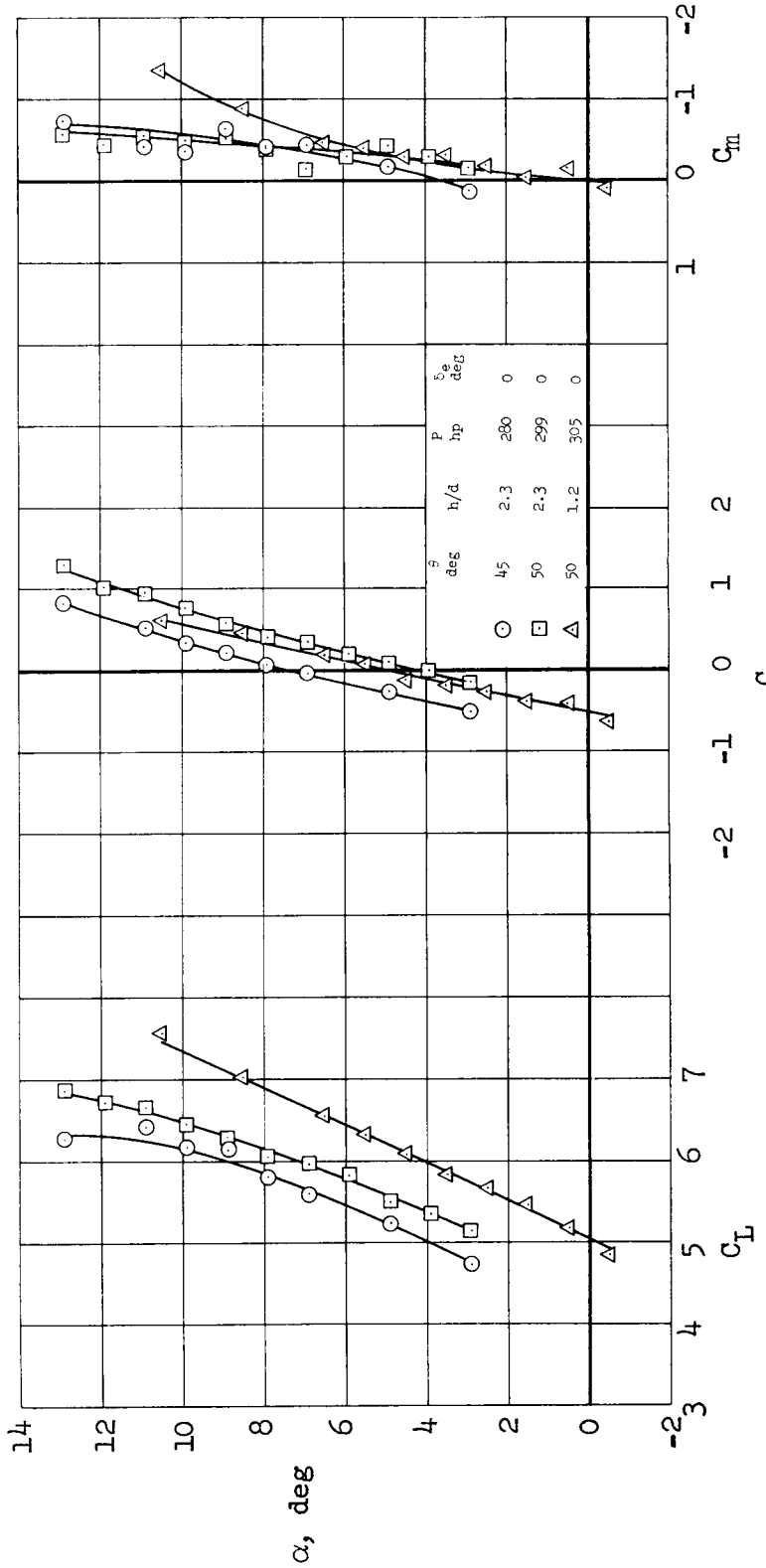

(c) V_∞ = 40 knots; $\theta_F = 31^\circ$.

Figure 9.- Continued.

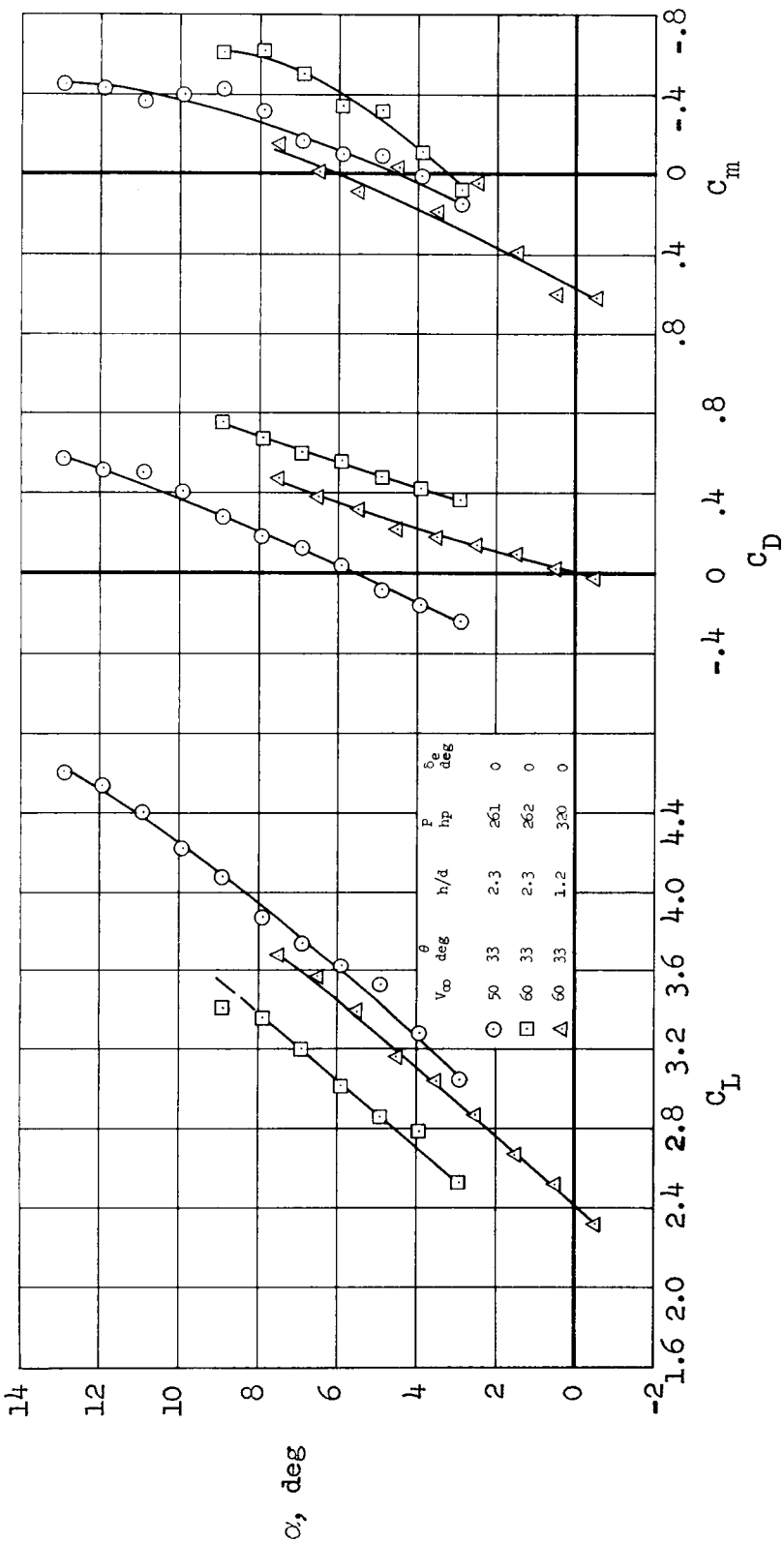

(d) V_∞ = 50 and 60 knots; $\theta_F = 31^\circ$.

Figure 9.- Concluded.

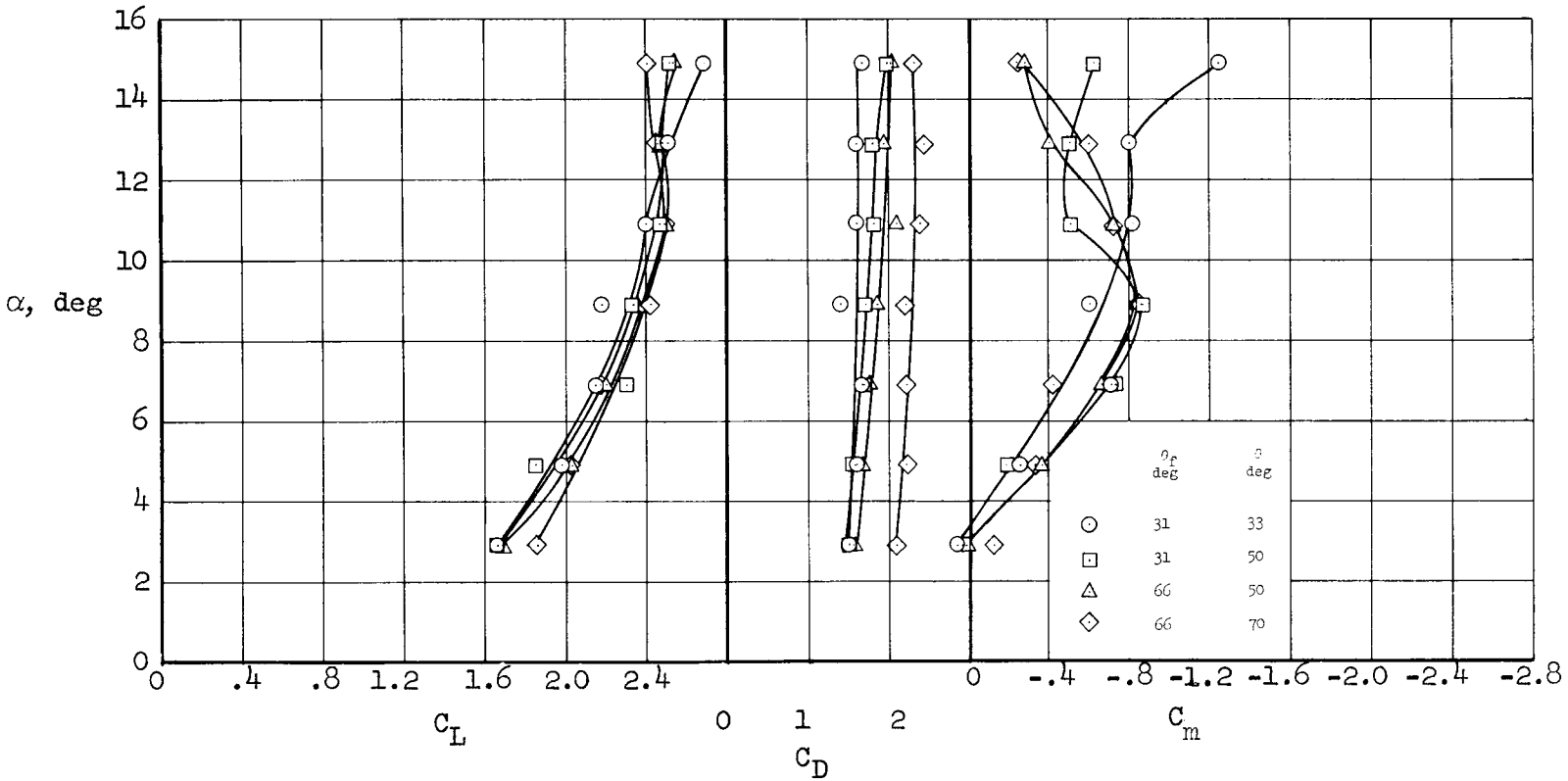

(a) h/d = 2.3

Figure 10.- Characteristics of the aircraft with power off and low-horizontal-tail position; $\delta_e = -5^\circ$.

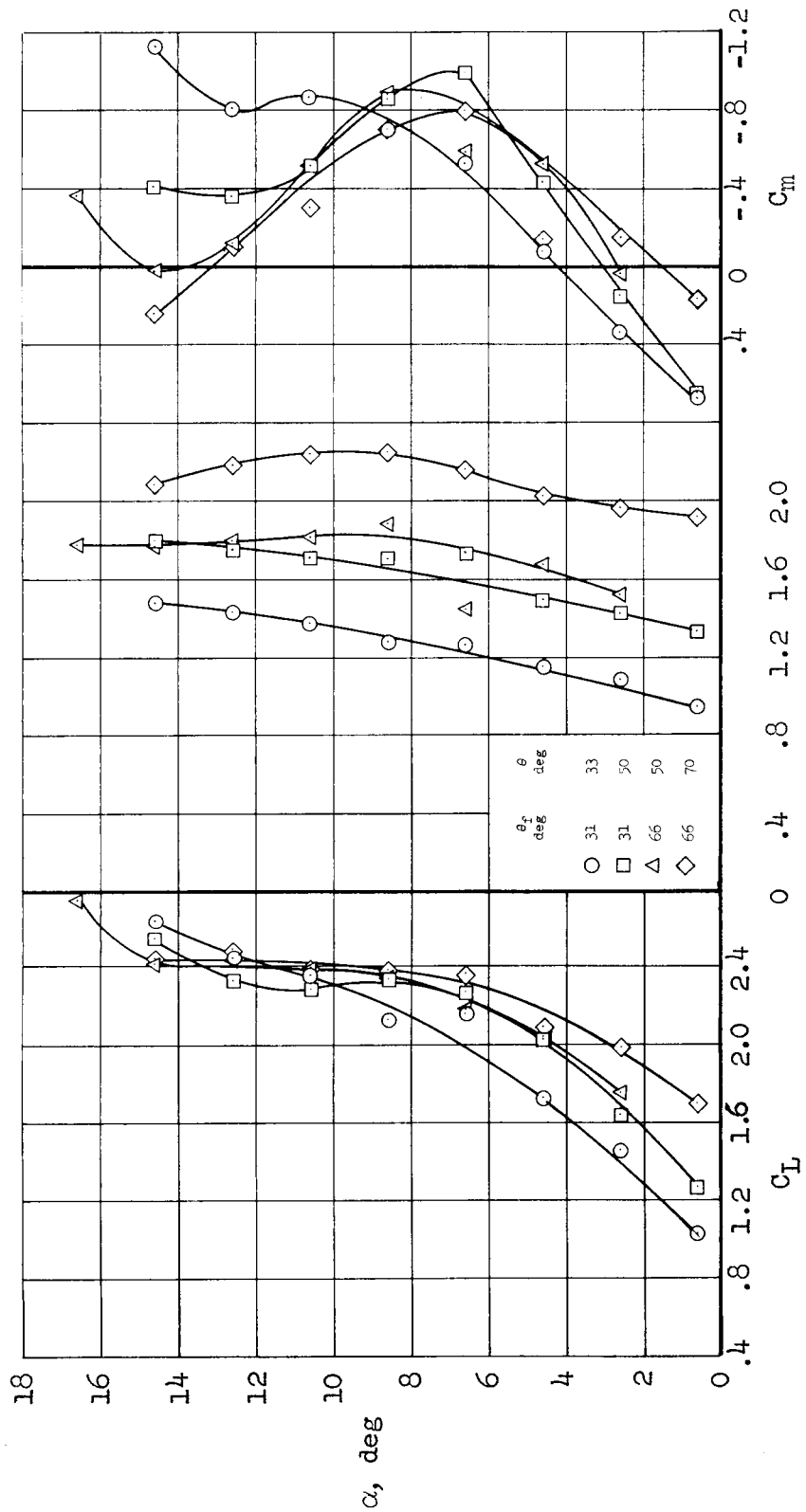

(b) h/d = 1.6

Figure 10.- Continued.

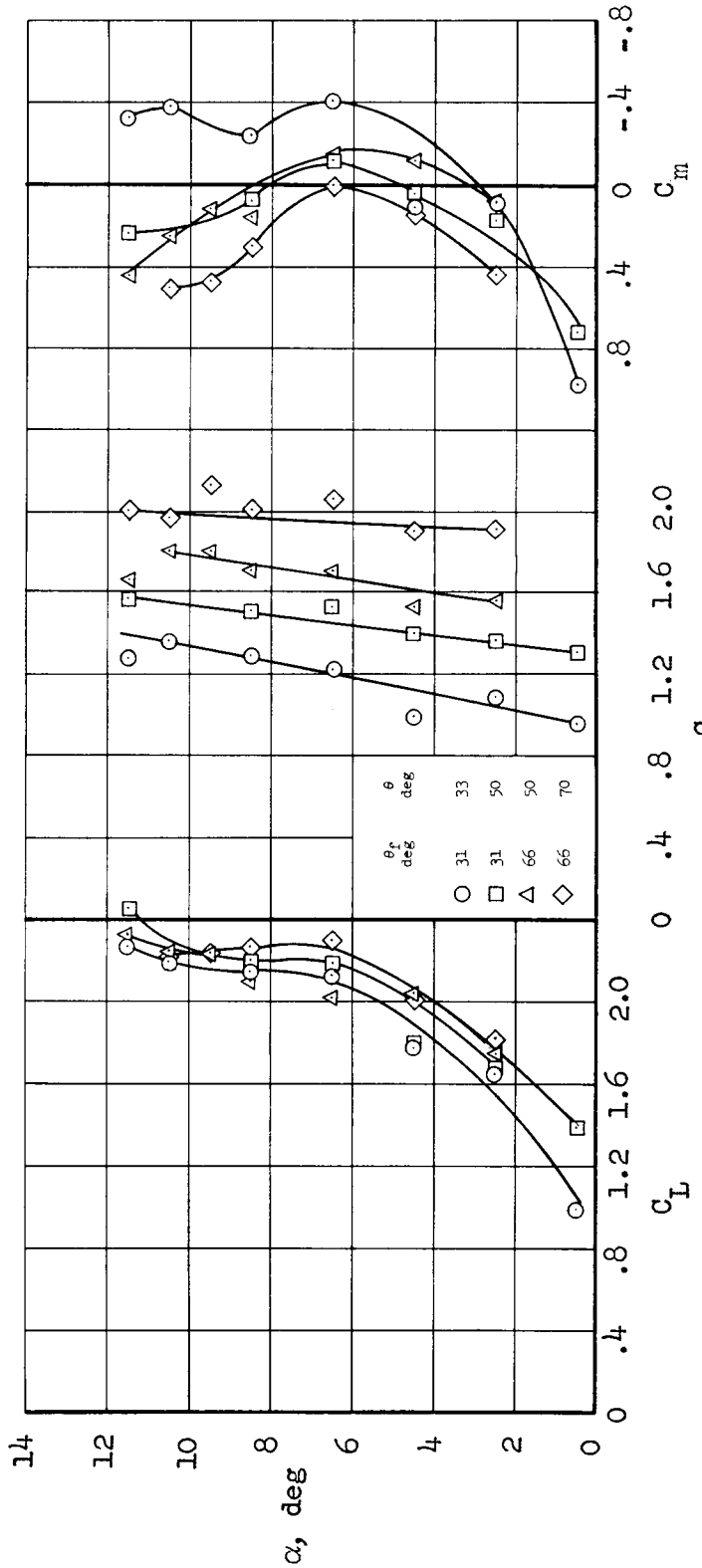

(c) h/d = 1.2

Figure 10.- Concluded.

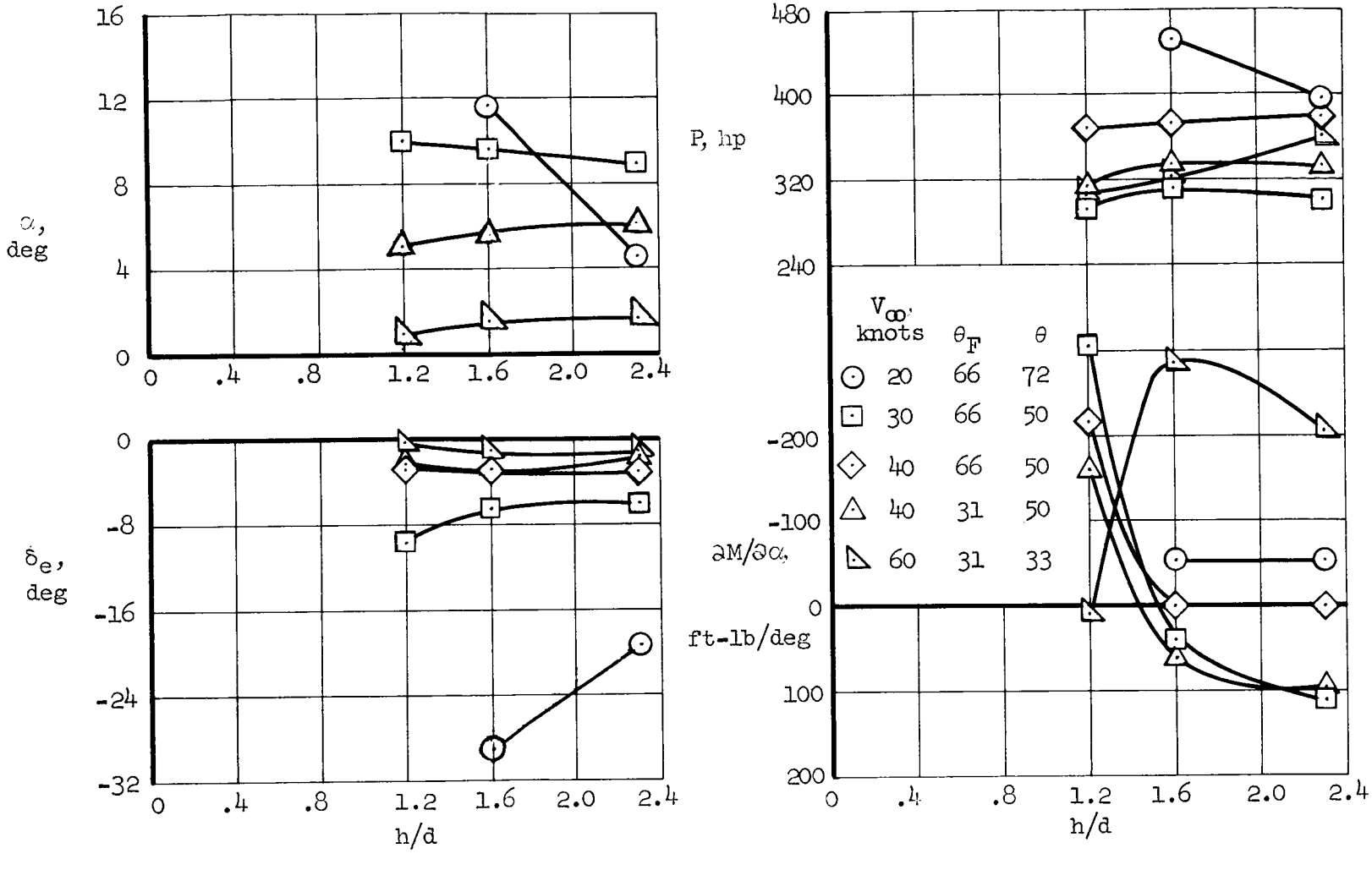

(a) Low-horizontal-tail position.

Figure 11.- Control and power settings necessary to trim for lift = 1500 pounds as a function of ground height.

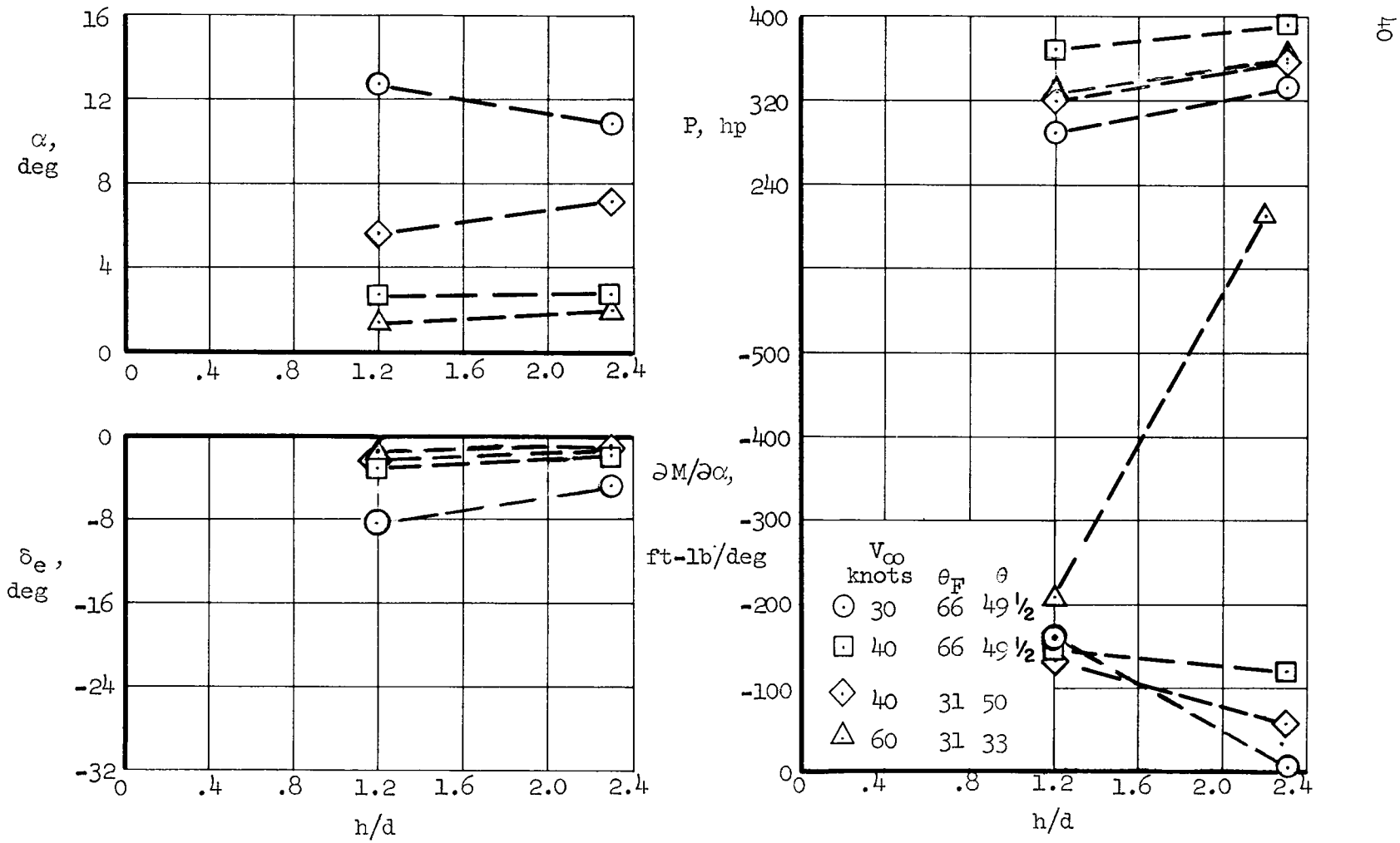

(b) High-horizontal-tail position.

Figure 11.- Concluded.

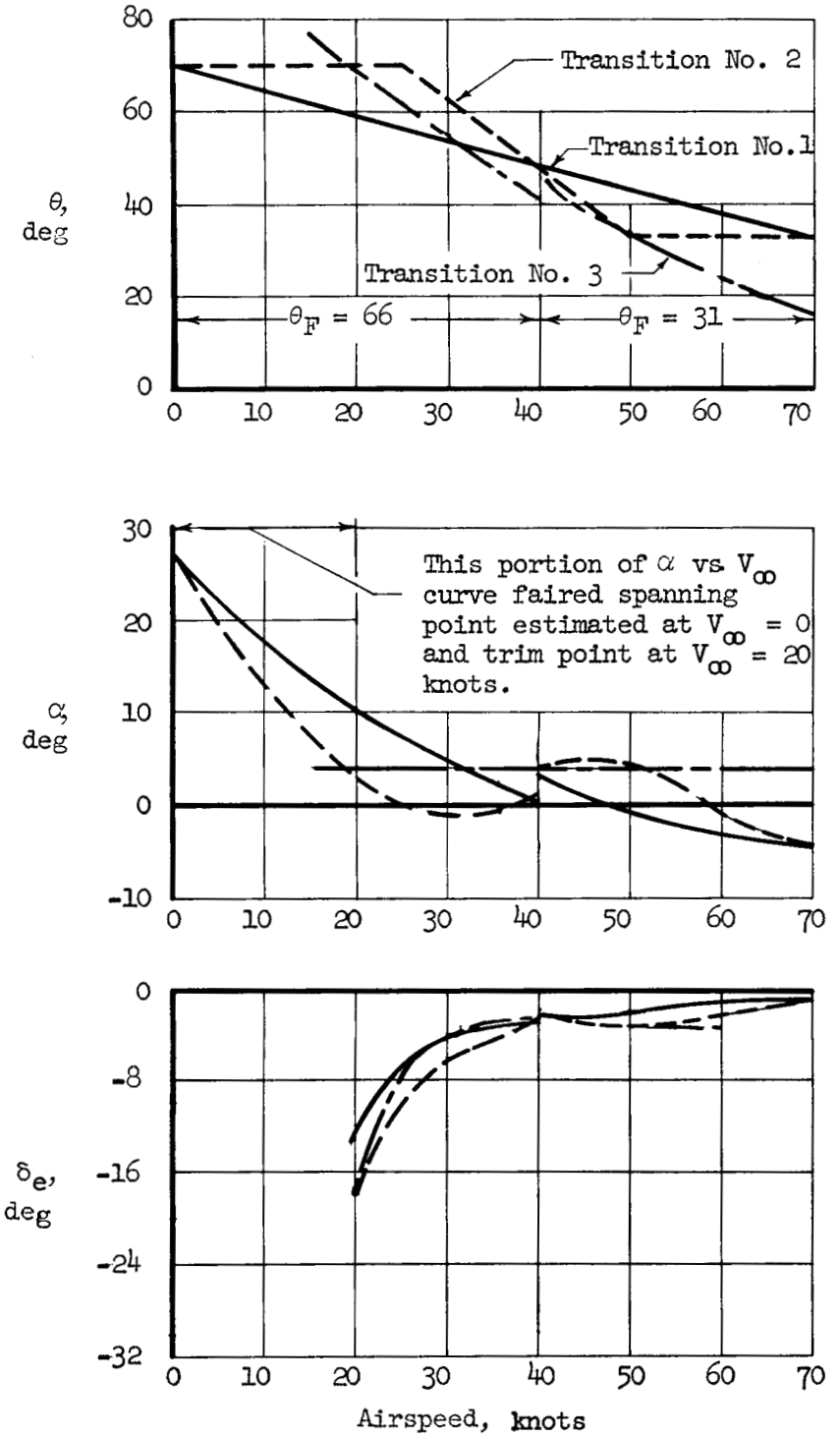

(a) θ, α, and δ_e vs. V_∞.

Figure 12.- Transition procedures from hovering to level forward flight; data from reference 3; low-horizontal-tail position.

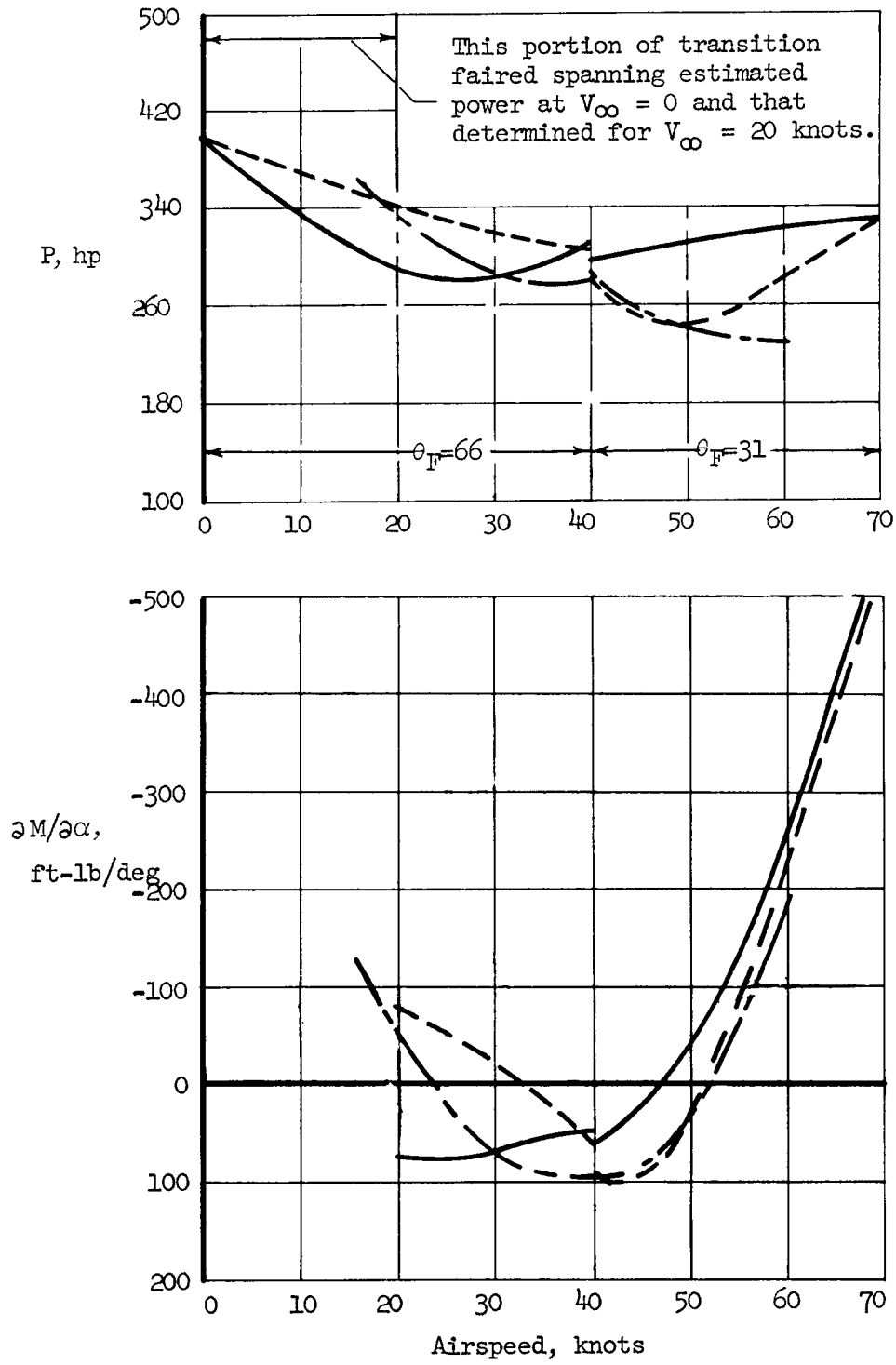

(b) P and $\partial M/\partial\alpha$ vs. V_∞

Figure 12.- Concluded.

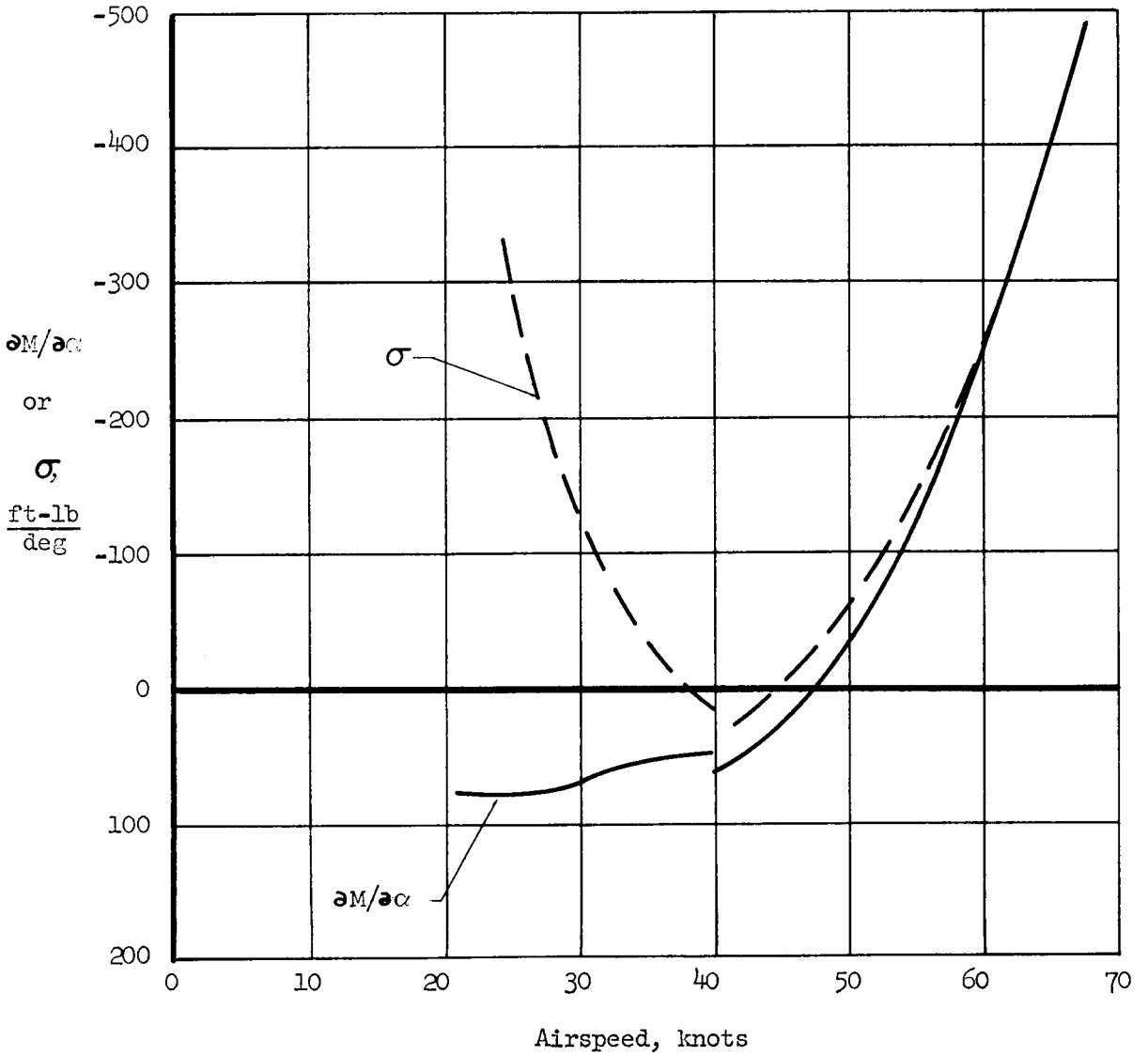

Figure 13.- The variation of longitudinal stability parameters with airspeed for transition no. 1.

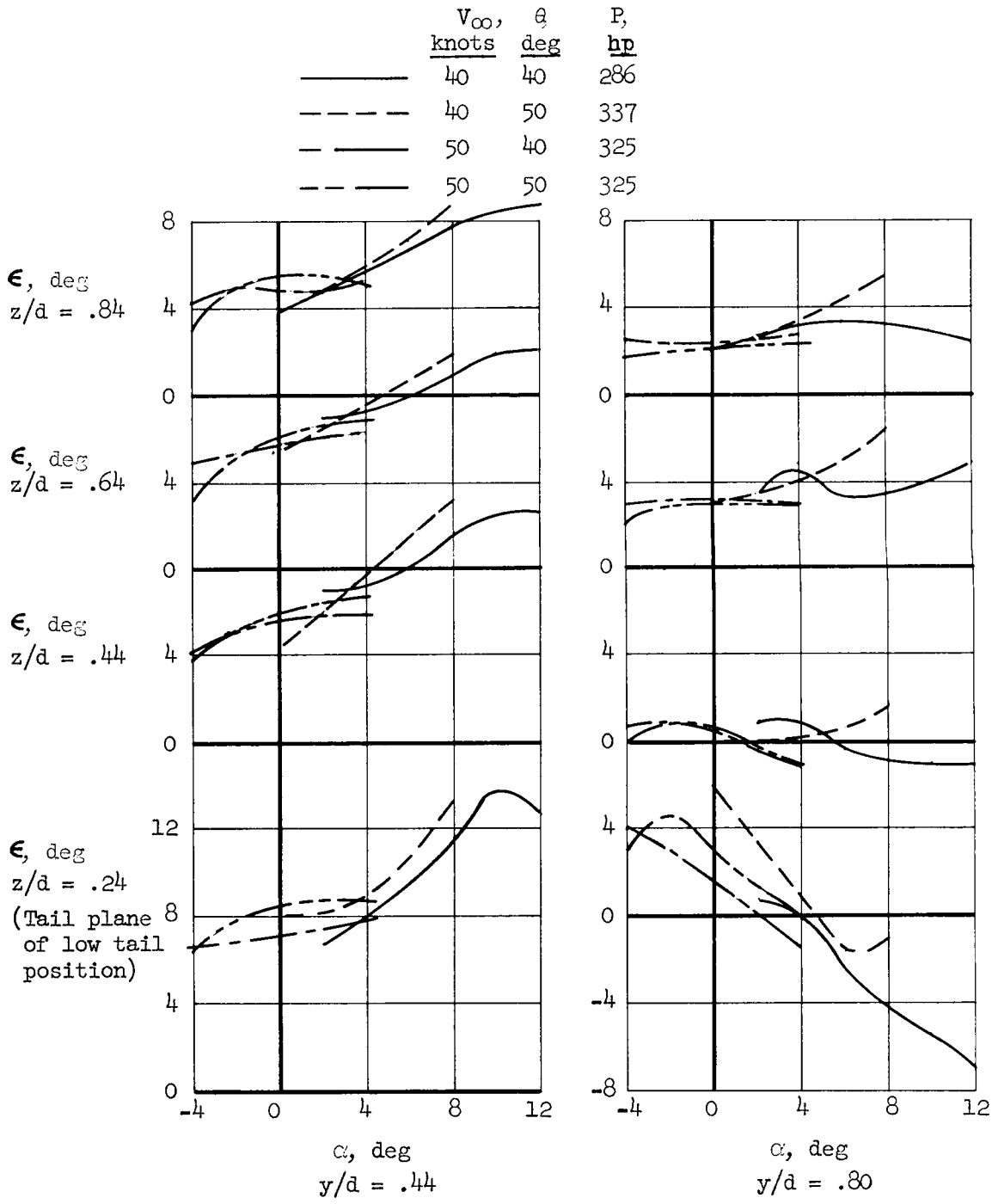

Figure 14.- Variation of downwash with angle of attack at several positions in the vicinity of the horizontal tail, from tests reported in reference 3.

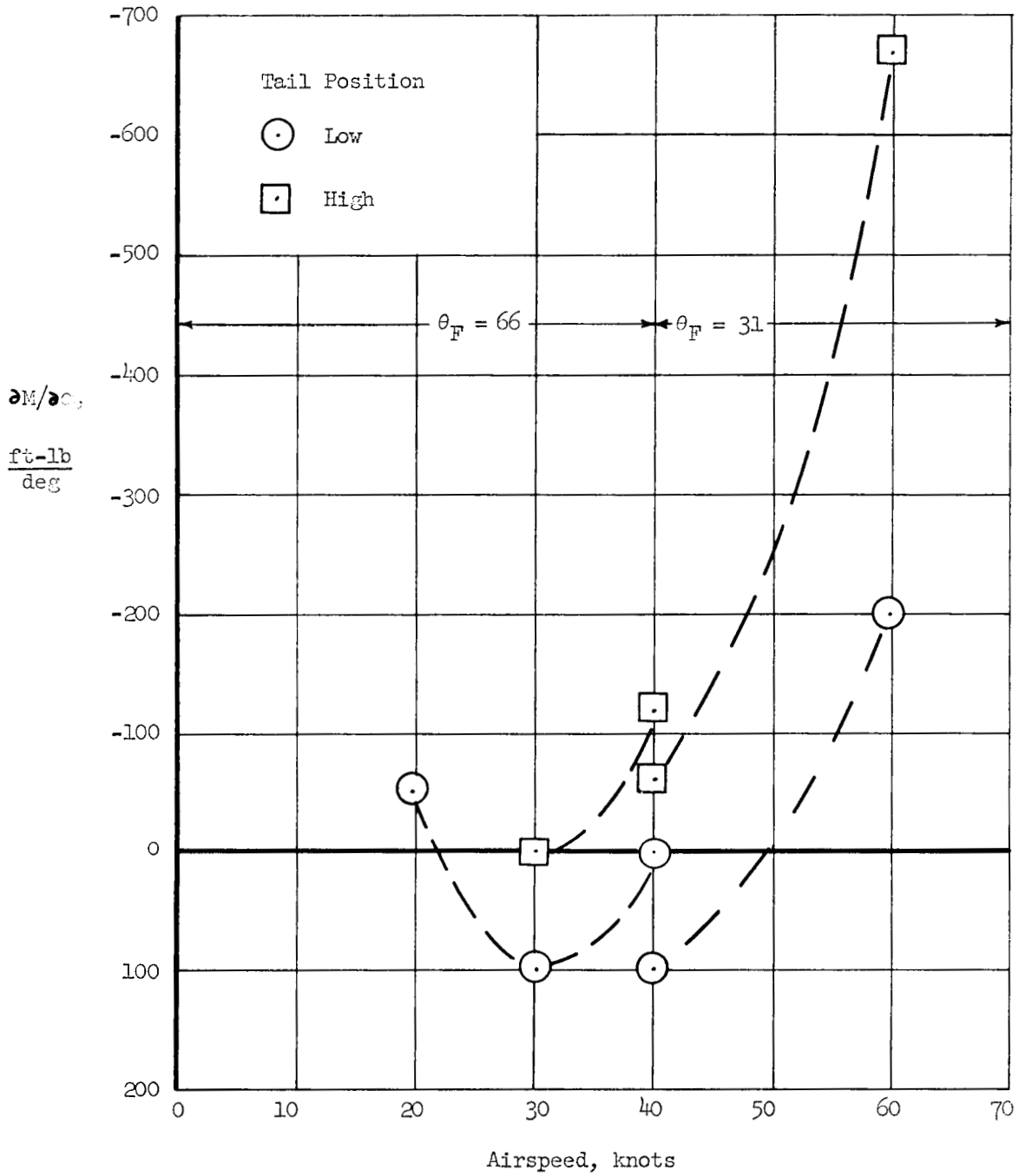

Figure 15.- The effect of horizontal tail height on the stability of the aircraft as indicated by $\partial M/\partial \alpha$; h/d = 2.3; θ, P, and δ_e varying to maintain trim at constant α.

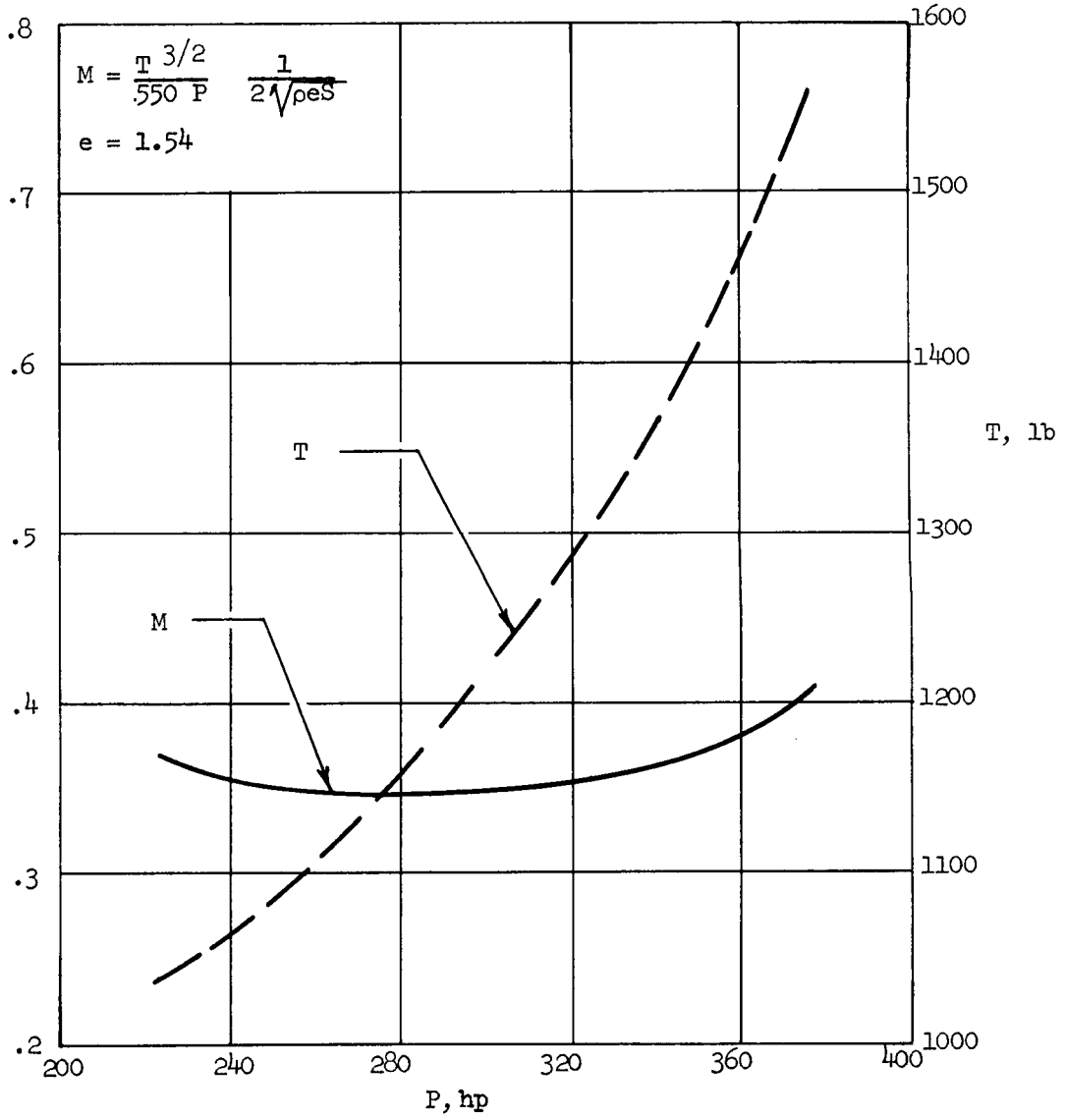

Figure 16.- Variation of figure of merit and static thrust with engine chart power; low tail position; wind-tunnel installation of reference 3.

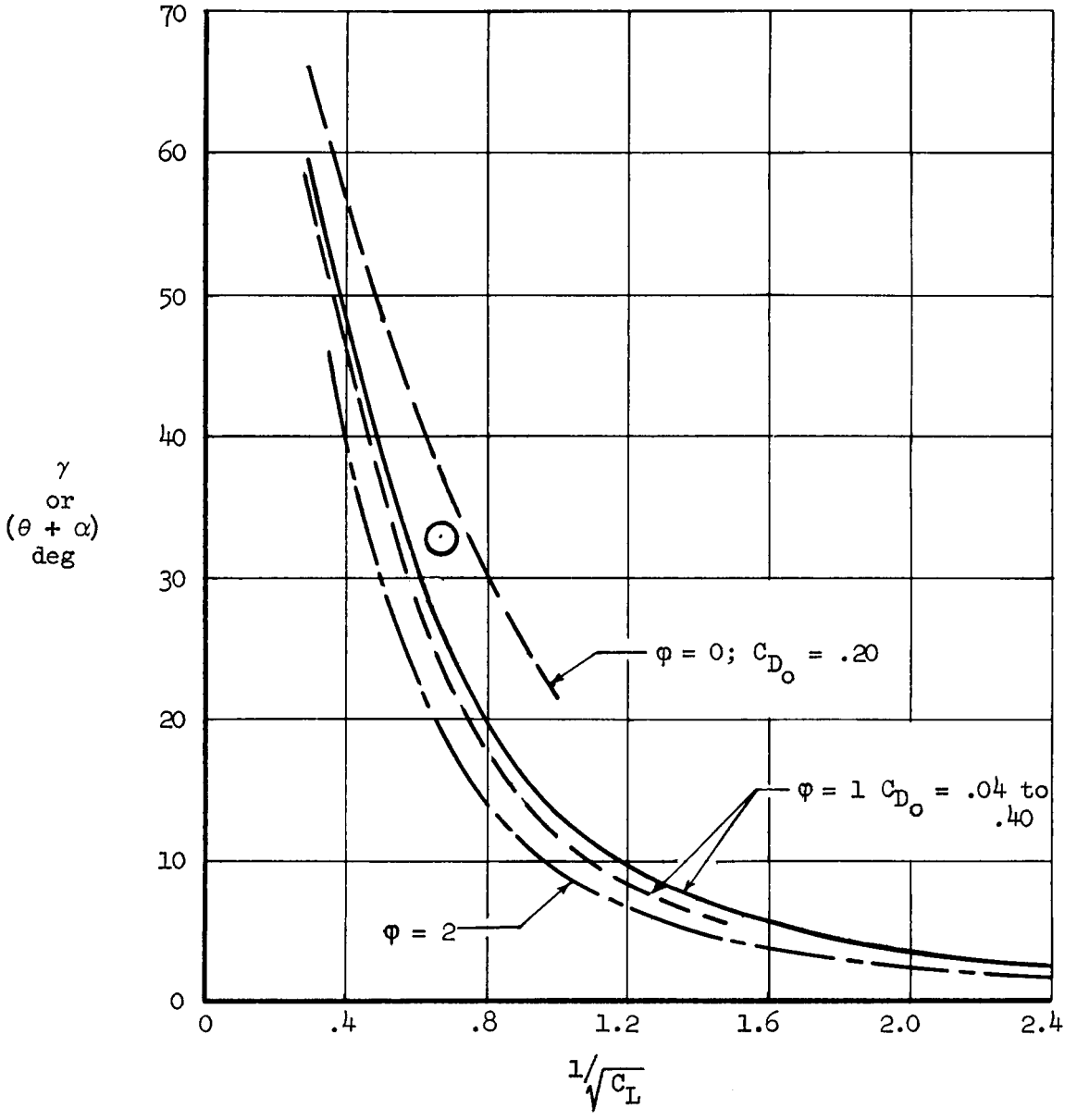

(a) Jet deflection angle vs. speed parameter.

Figure 17.- Forward flight performance of the aircraft; faired curves represent the theory of references 1 and 2; the test point was derived from data of reference 3 for the aricraft with horizontal tail off; $V_\infty = 60$ knots; $\alpha = 0$.

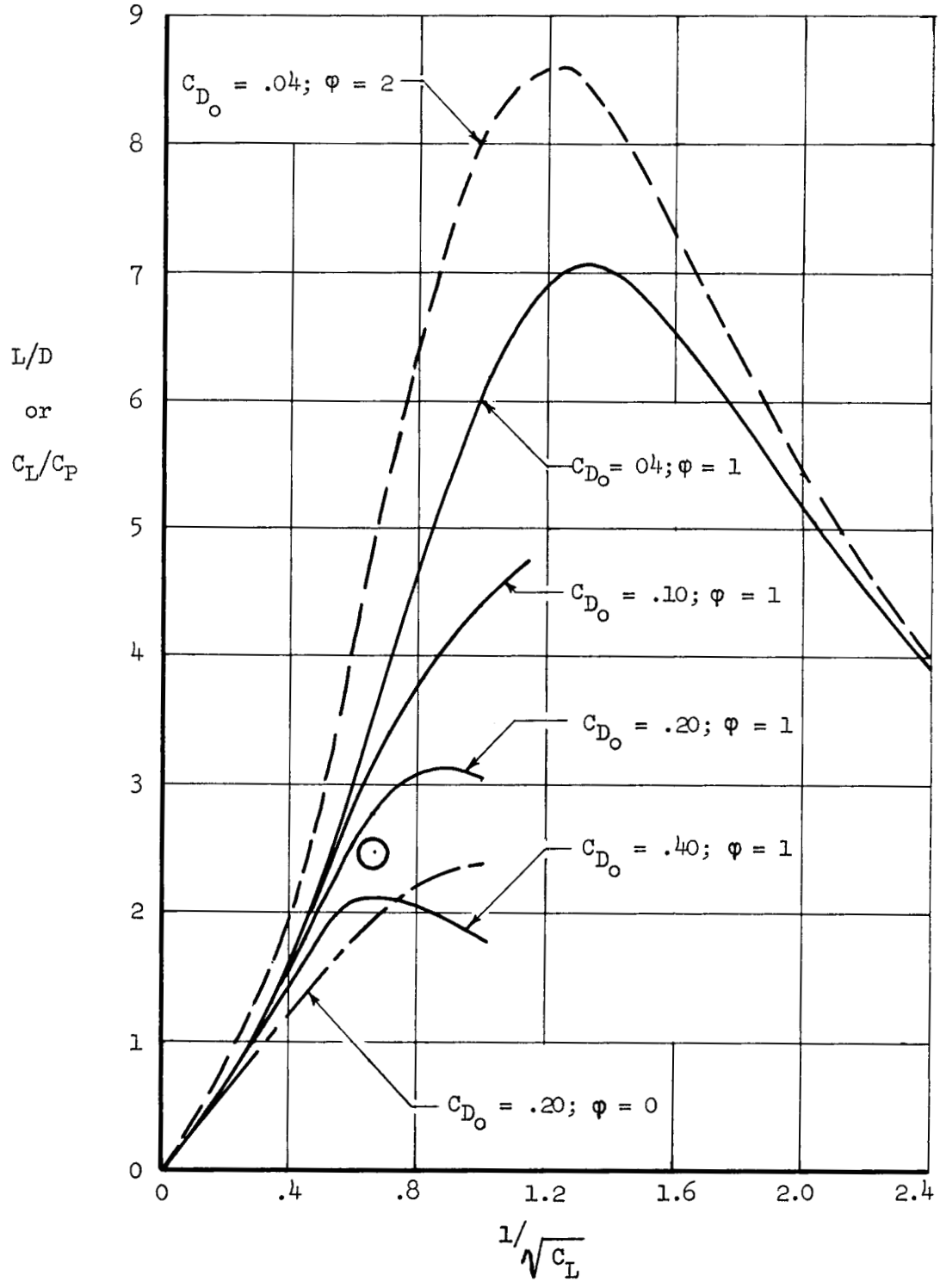

(b) L/D vs. speed parameter.

Figure 17.- Concluded.